Synthesis and biological evaluation of a new class of benzothiazines as neuroprotective agents

Synthesis and Biological Evaluation of a New Class of Benzothiazines as Neuroprotective Agents

Alessandra Mancini,[a] Alessia Chelini,[a] Angela Di Capua,[a,b] Loretta Castelli,[c] Simone Brogi,[a] Marco Paolino,[a] Germano Giuliani,[a] Andrea Cappelli,[a] Maria Frosini,[d] Lorenzo Ricci,[d] Erminia Leonelli,[d] Gianluca Giorgi,[a] Antonio Giordani,[e] Jacopo Magistretti,[c] and Maurizio Anzini[a,]*

[a]*Dipartimento di Biotecnologie, Chimica e Farmacia Università di Siena, Via A. Moro, 53100 Siena, Italy*
[b]*Eskitis Institute for Drug Discovery, Griffith University, Brisbane, Queensland, Australia*
[c]*Dipartimento di Biologia e Biotecnologie, Fisiologia Generale, Università di Pavia, Via Forlanini 6, 27100 Pavia, Italy*
[d]*Dipartimento di Scienze della Vita, Università di Siena, Via A. Moro, 53100 Siena, Italy, and eRottapharm Biotech, Via Valosa di Sopra 7, 20052 Monza, Italy*

*Corresponding author. Tel. +390577 234173; fax +39 0577 234254; e-mail: maurizio.anzini@unisi.it

Abstract

Neurodegenerative diseases are disorders related to the degeneration of central neurons that gradually lead to various, severe alterations of cognitive and/or motor functions. Currently, for no such diseases does any pharmacological treatment exist able to arrest its progression. Riluzole (**1**) is a small molecule able to interfere with multiple cellular and molecular mechanisms of neurodegeneration, and is the only approved treatment of amyotrophic lateral sclerosis (ALS), the progression of which proved able to significantly slow, thus increasing somewhat average survival. Here we report the synthesis of differently functionalized 4*H*-3,1-benzothiazine (**5**-**6**) and 2*H*-1,4-benzothiazine (**7**) series as superior homologues of **1**. Biological evaluation demonstrated that amidine 4*H*-3,1-benzothiazine derivatives **5b**-**d** can reduce glutamate and LDH release in the oxygen/glucose deprivation and reperfusion model (OGD/R) applied to brain slices with a higher potency than **1**. Moreover the mentioned compounds significantly reduce glutamate- and 6-hydroxydopamine (6-OHDA)-induced cytotoxicity in neuroblastoma cells. In addition, the same compounds limit ROS formation in both neuronal preparations. Finally, **5c** proved effective in inhibiting neuronal voltage-dependent Na^+ and Ca^{2+}-channels, showing a profile comparable with that of **1**.

Keywords: Neuroprotective Agents, Neurodegenerative Diseases, Benzothiazine derivatives, SH-SY5Y cells, Neuronal Voltage-Dependent Na^+ and Ca^{2+} Currents

1. Introduction

Chronic neurodegenerative disorders, such as Alzheimer's disease (AD), Parkinson's disease (PD), Huntington's disease (HD), and amyotrophic lateral sclerosis (ALS), as well as acute neurodegenerative diseases like brain ischemia, represent severe pathologies in developed world. The impact of of these neurodegenerative diseases is dramatically increased due to the society ageing , with huge human and economic costs [1]. Currently, the pathogenesis of the mentioned disorders is not fully understood, and none of the currently available treatments can stop their progression. In this scenario, it is claimed that the administration of drug(s able to modulate multiple pathways involved in the onset and progression of the pathology may slow and definitely stop the evolution of the disease itself [2]. The aetiology of different neurodegenerative diseases, however, is a complex process involving conjoint genetic and cellular mechanisms, which dynamically interact to cause a common final, neurodegenerative outcome [3]. In particular, several experimental data strongly suggest that excitotoxic-mediated neuronal damage plays a crucial role in the early pathogenesis of chronic as well as acute neurodegenerative diseases [4]. Over-activation of glutamate receptors impairs cellular calcium homeostasis with consequent activation of neuronal nitric oxide synthase (*n*NOS). Nitric oxide (NO) overproduction generates free radicals and programmed cell death. Simultaneous inhibition of key signals involved in excitotoxic cell death will provide interesting and efficacious potential approaches for therapeutic intervention. This can be attained either by means of a combination of drugs each endowed with different mechanisms of action, or by means of multi-target-direct ligands[5-6].

Since each step of the excitotoxic cascade represent an attractive target for the development of neuroprotective agents beneficial for the treatment of many chronic and acute brain diseases we developed new compounds endowed with neuroprotective activity and particularly focused on those potentially useful in the treatment of ALS. Our attention was firstly attracted by riluzole (**1**, 2-amino-6-

(trifluoromethoxy)benzothiazole) (Figure 1), which has been shown to possess neuroprotective effects in animal models of PD [7], HD [8] and cerebral ischemia [9].

Interestingly, **1** is a small molecule (MW = 234.2) that *in vitro* may elicit multiple molecular actions, among which those clinically relevant are inhibition of voltage-gated sodium channels [10-13], which can lead to reduced neurotransmitter release, non-competitive inhibition of NMDA receptors [14-15], inhibition of glutamate release [16], and enhanced astrocytic uptake of extracellular glutamate [17].

Currently, **1** is the only drug that has proved able to modify the course of ALS [18-20] and the only one approved for the treatment of this disease.

On these bases we designed and reported [21, 22] the synthesis and the biological evaluation of amidine and guanidine derivatives **2** and **4**, respectively (Figure 1), as **1**-like compounds with the aim of conjugating the neuroprotective effects of **1** with the neuroprotective and anti-inflammatory activity of 1400W [23] and the NOS-inhibiting properties of aminoguanidine [24] and L-NAME [25] (Figure 1). Thiourea derivatives **3** (Figure 1) were synthesized because many thioureas were found to be potent free radical scavengers able to prevent oxidative damage [26].

Derivatives **2**-**4** were tested using an *in vitro* protocol of ischemia/reperfusion injury and the results revealed that **2c** and **3a-d** meaningfully reduced neuronal injury. In particular, compounds **3a-d** were selected for evaluating their antioxidant properties. The results proved that the mentioned compounds were endowed with a direct ROS scavenging activity. Compounds **3b** and **3d** underwent electrophysiological studies on voltage-dependent Na^+ and Ca^{2+} currents in neurons from rat piriform cortex. Compound **3b** , inhibited the transient Na^+ current at 50 μM but to a much smaller extent than **1** [22].

Encouraged by our results we decided to pursue the synthesis of two different series of benzothiazines **5-7** (Figure 2), as cyclic homologation of benzothiazole**.**.

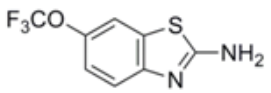

riluzole (**1**)

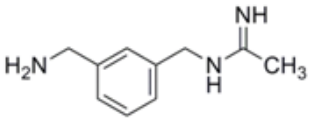

1400W

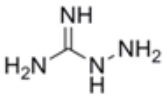

aminoguanidine

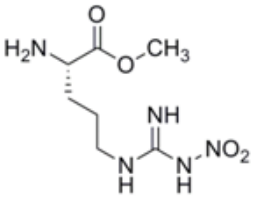

L-NAME

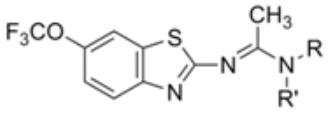

2

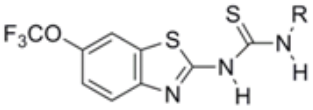

3

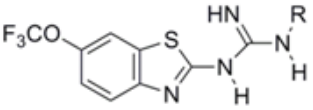

4

	R	R'
2a	H	H
2b	H	Me
2c	Me	Me
2d	Et	Et
2e	*n*-Pr	*n*-Pr

	R
3a	Et
3b	*n*-Pr
3c	*i*-Pr
3d	*n*-Bu
3e	Ph
3f	4-F-C_6H_4

	R
4a	Et
4b	*n*-Pr

Figure 1. Reference compounds.

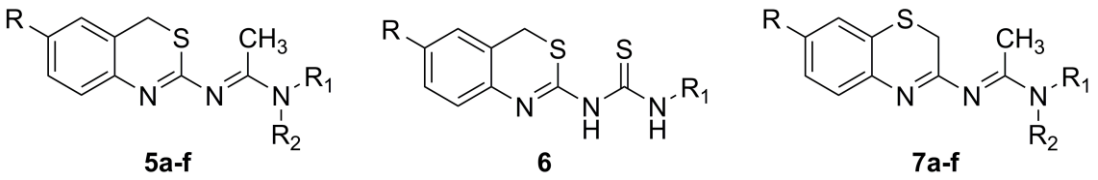

Compound	R	R_1	R_2
5a	H	Me	H
5b	H	Me	Me
5c	H	Et	Et
5d	H	*n*-Pr	*n*-Pr
5e	OCF_3	Et	Et
5f	OCF_3	*n*-Pr	*n*-Pr
6	H	*n*-Pr	-
7a	H	Me	H
7b	H	Me	Me
7c	H	Et	Et
7d	H	*n*-Pr	*n*-Pr
7e	OCF_3	Et	Et
7f	OCF_3	*n*-Pr	*n*-Pr

Figure 2. Structures of target compounds **5**-**7**.

2. Results and Discussion

2.1. Chemistry

The synthesis of 2-amino-4*H*-3,1-benzothiazines **15** and **16** has been accomplished as reported in Scheme 1. The protection of the amino group of *p*-trifluoromethoxyaniline **8** by means of pivaloyl acid chloride in the presence of Et_3N gave pivaloyl amide **9** [27] that was in turn formylated with *t*-BuLi and dry DMF to afford aldehyde **10**. Reduction of this compound with $NaBH_4$ in EtOH gave benzyl alcohol **11** that, by treatment with concentrated HCl in dioxane, was transformed into the corresponding chloromethyl derivative and contemporary deprotected to yield 4-trifluorometoxyaniline **12**. The condensation of compound **12** with thiourea in isopropyl alcohol

afforded the expected 2-amino-6-trifluorometoxy-4*H*-3,1 benzothiazine **15**. As for the synthesis of unsubstituted 2-amino-4*H*-3,1-benzothiazine **16**, 2-aminobenzyl alcohol **13** was used as the starting material, and subjected to the same reactions used for the *o*-trifluorometoxy derivative **15**. The transformation of benzyl alcohol **13** into chloromethyl derivative **14** and successive cyclization with thiourea yielded compound **16** in quantitative yield [28].

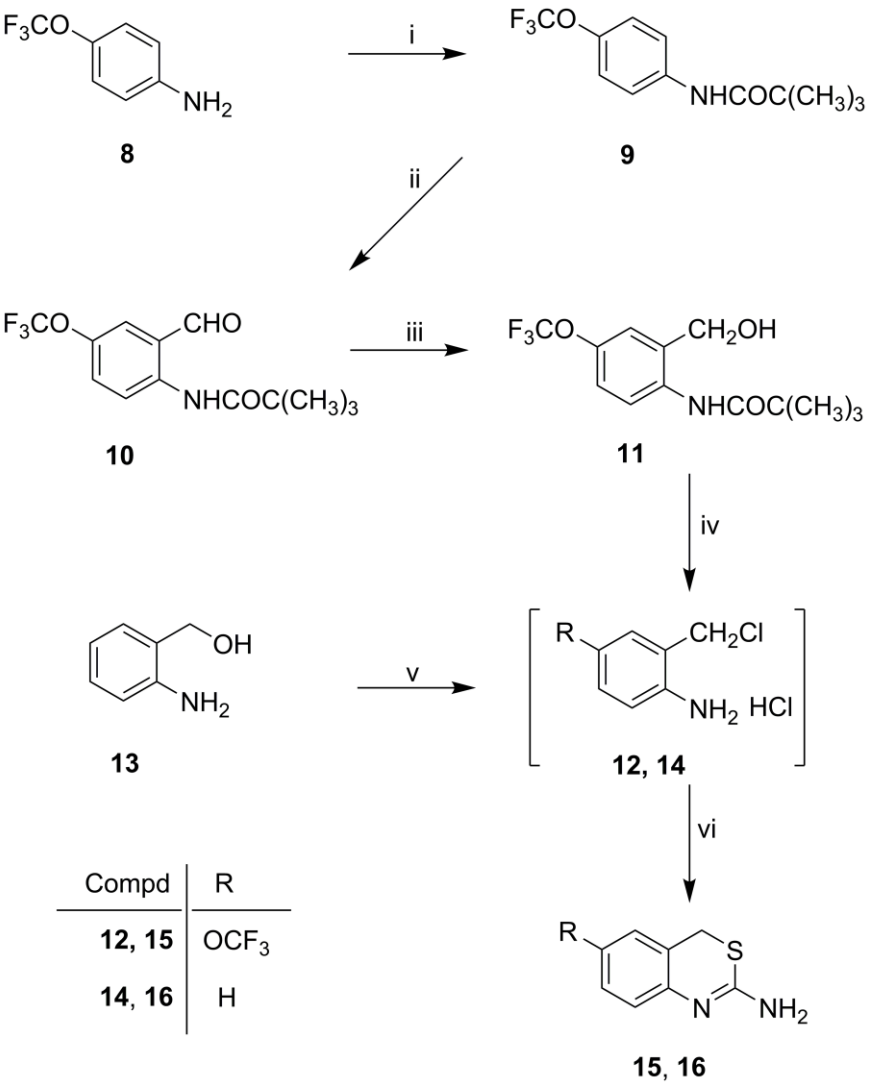

Scheme 1. Reagents: (i) $(CH_3)_3CCOCl$, Et_3N, CH_2Cl_2; (ii) *t*-BuLi, dry THF, dry DMF; (iii) $NaBH_4$, absolute EtOH; (iv) HCl 37%, dioxane; (v) HCl 37%, sealed vial; (vi) NH_2CSNH_2, i-PrOH.

o-Amino-*S*-cyanomethylthiophenol **18** used for the preparation of 3-amino-7-trifluoromethoxy-2*H*-1,4-benzothiazine **19** was prepared by hydrolysis of **1** followed by alkylation with chloroacetonitrile in

the presence of $(Bu)_4N^+HSO_4^-$ and 10 M NaOH. Compound **18** was readily cyclized by refluxing in ethanolic HCl (5%) to give the desired compound **19**. As for the synthesis of unsubstituted 3-amino-2*H*-1,4-benzothiazine **21** the *o*-aminotiophenol **20** was used as the starting material and subjected to the same alkylation and cyclisation procedures as reported above to afford the expected compound **21** [29] (Scheme 2).

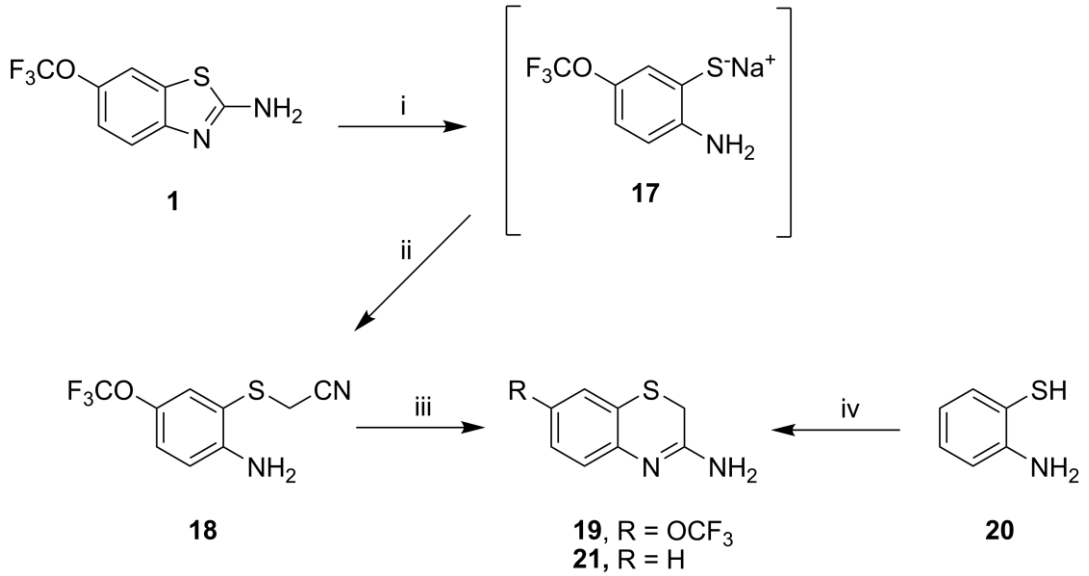

Scheme 2. Reagents: (i) NaOH 10 M; (ii) $ClCH_2CN$, $(Bu)_4N^+HSO_4^-$, NaOH 10 M, CH_2Cl_2; (iii) HCl/EtOH 5%; (iv) $ClCH_2CN$, $(Bu)_4N^+HSO_4^-$, NaOH 25%, CH_2Cl_2.

Compound **1**, used to prepare compound **19**, is quite expensive, then we decided to prepare it in house according to an already published procedure (Scheme 3) [30]. Briefly, **1** was prepared via one-pot procedure based on the condensation of **8** with 1 molar equivalent of ammonium thiocyanate and benzyltrimethylammonium tribromide in CH_3CN as described in literature [30] (but in better yields, 80%).

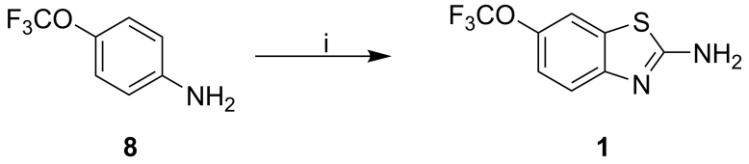

Scheme 3. Reagents: (i) NH_4SCN, $PhCH_2N(CH_3)_3Br_3$, CH_3CN.

Compounds **15**, **16**, **19**, and **21** were transformed into the corresponding amidines **5a-f**, **7a-f** and thiourea **6**, respectively, according to well-established methodologies (Scheme 4) [22,31].

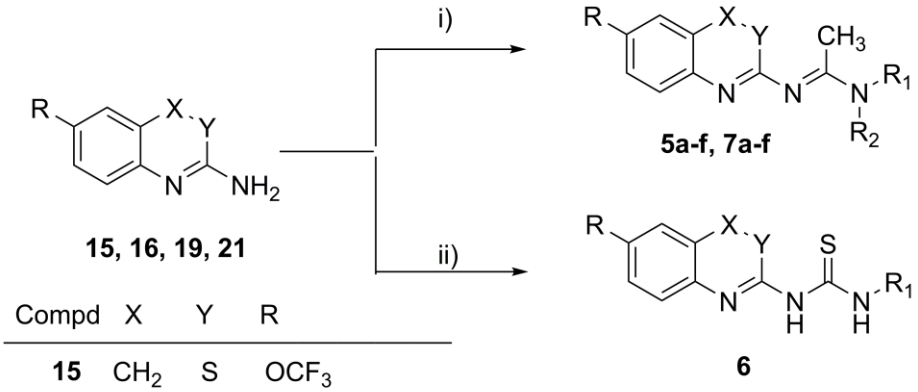

Compd	X	Y	R
15	CH_2	S	OCF_3
16	CH_2	S	H
19	S	CH_2	OCF_3
21	S	CH_2	H

Scheme 4. Reagents: (i) $CH_3CONR_1R_2$, $POCl_3$, dry toluene; (ii) R_1NCS, Et_3N, dry toluene. R_1 is defined in Figure 2.

2.2. Biological evaluation

The neuroprotective properties of the compounds reported in Table 1 were first investigated by means of rat brain slices, an experimental model that preserves the exact cellular architecture of an intact brain and that can be used for an appropriate and accurate extrapolation of findings in terms of neuroprotection. Since excitotoxicity is a key step of the ischemic cascade, which lead to neuronal loss, rat brain slices were exposed to ischemia-like condition (oxygen glucose deprivation and reperfusion, OGD/R). The amount of LDH and glutamate release from the tissue to the medium was taken as an index directly related to tissue damage and inversely related to neuroprotection. Compounds were added after the injury since, from a clinical point of view, this is more relevant than a treatment performed before the damage, being neurodegeneration almost unpredictable. Results demonstrated that among the newly tested compounds **5b**,**d** were the most effective in reverting OGD/R-induced LDH and glutamate release. As observed for **1** [22], however, their effects followed a U-shaped, hormetic-like concentration-response curve (Figure 3).

For LDH release, the efficacy window was 0.01-0.1 μM for **5b** or 0.1-5 μM for **5c** and **5d**, while the minimal effective concentration (MEC) was 0.01 μM and 0.1 μM, respectively, i.e. values that differ by one or two orders of magnitude from that of **1** (1 μM). These derivatives had a maximum effect of about 78% (**5b**) and concentrations higher than the efficacy window were less active or ineffective in exerting neuroprotection. Regarding the ability of the tested compounds to counteract OGD/R-induced glutamate release, **5c** and **5d** had a wider efficacy window than **1**, and they also effectively reverted glutamate release at a concentration of 0.1 μM (**5c**) or 1 μM (**5d**), respectively.

5a, **7a**, **7d**, **15**, and **6** were less active than **1** and the above-mentioned compounds. In particular, **15** and **6** partially reverted glutamate release (~ 50-60%) and, at the same time, did not modify that of LDH. This can be explained by considering the possibility that **15** and **6** could hamper the steps of ischemic cascade that lead to glutamate release into the extracellular space without affecting those which lead to neuronal death. **7a** and **7d** exert poor neuroprotection since they partially reverted the

release of the endocellular enzyme into the medium, leaving that of glutamate unchanged **7d** or only moderately reduced (i.e. **7a)**. Compounds **7b**,**c** and **5e**, however, showed no activity.

Table 1. Effects of **1** and compounds **5e-f**, **6b**, **7a-d** and **15** on OGD and reperfusion-induced release of glutamate (GLU) and LDH in rat cortical brain slices.

Compounds	**GLU**		**LDH**	
	Efficacy window[a] (μM)	MEC[b] (% ± SEM)[c]	Efficacy window (μM)	MEC (% ± SEM)
1 Riluzole[d]	1.0-25	1 (100)	0.1-100	10.0 (100.0 ± 4.5)
5a	5.0-50	5 (43.6 ± 5.7)	1	0.1 (40.1 ± 5.3)
5b	0.01-0.1	0.01 (72.7 ± 10.3)	0.01-1.0	0.01 (78.4 ± 2.7)
5c	0.1-25.0	0.1 (100.0 ± 4.4)	0.1-5.0	0.1 (72.4 ± 5.9)
5d	0.1-25.0	1 (90.5 ± 3.6)	0.1-1.0	0.1 (58.2 ± 3.8)
5e	N.E.	N.E.	N.E.	N.E.
5f	0.01-1.0	0.01 (17.8 ± 5.8)	0.1	0.1 (31.0 ± 2.1)
6b	0.001	0.001 (45.7 ± 8.9)	N.E.	N.E.
7a	0.1-100	0.1 (25.5 ± 6.8)	100	100 (33.2 ± 9.2)
7b	N.E.	N.E.	N.E.	N.E.
7c	N.E.	N.E.	N.E.	N.E.
7d	N.E.	N.E.	10	10 (53.5 ± 5.7)
15	0.001-0.1	0.001 (69.1 ± 6.8)	N.E.	N.E.

[a]The efficacy windows represent the interval of concentrations at which a significant reduction of OGD-induced GLU and LDH release was observed. [b]MEC (Minimal Effective Concentration) is the μM concentration at which the highest reduction was observed. [c]The value between parentheses represents the % of reversion exerted at such concentration; 100% was taken as the return to basal values (CTRL). N.E.: inactive. [d]Data from ref. [22].

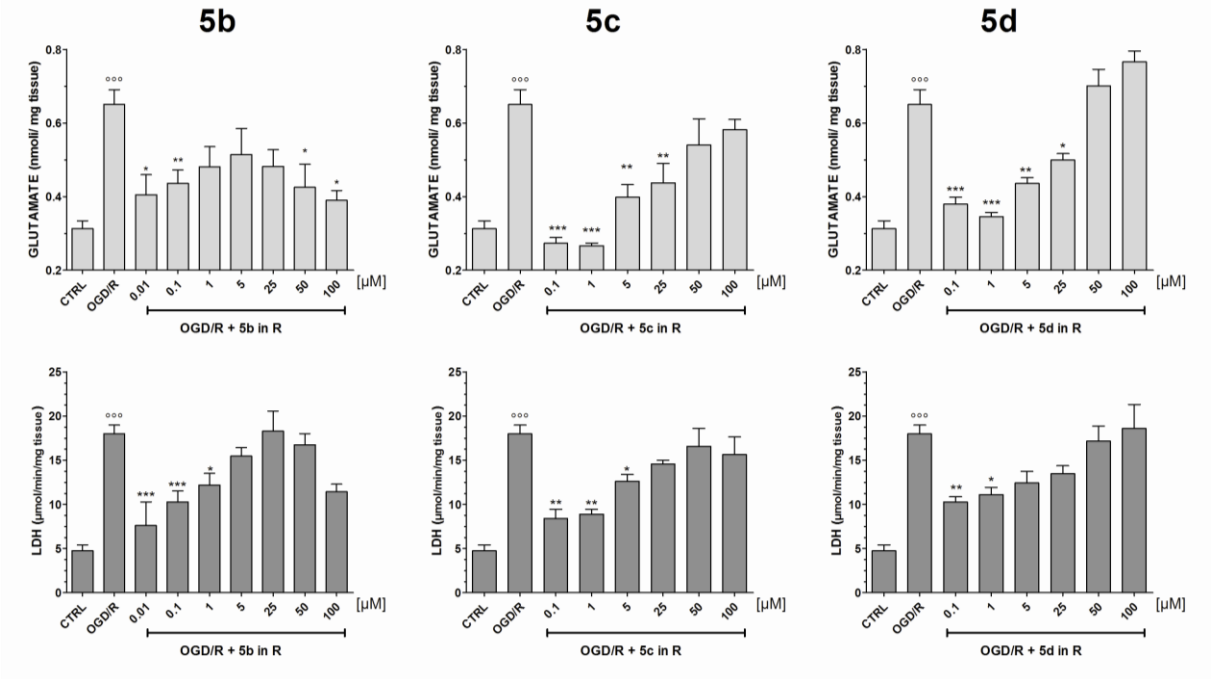

Figure 3. Effects of compounds **5b**, **5c** and **5d** on the release of glutamate and LDH induced by oxygen/glucose deprivation and reoxygenation (OGD/R) in rat cortical slices. Drugs were added to reoxygenation buffer used after OGD. Data are mean ± SEM of at least four different experiments. Statistical analysis was performed by applying ANOVA followed by a post hoc Dunnett test. °°°$p <$ 0.01 *vs* controls (CTRL). *$p < 0.05$, **$p < 0.01$, ***$p < 0.001$ *vs* OGD/R.

To further characterize the neuroprotective effects exerted by the most interesting compounds (**5b-d**) at the cellular level, the human neuroblastoma cell line, SH-SY5Y, widely employed in studies related to neurotoxicity, oxidative stress and neurodegenerative diseases [32,33]. SH-SY5Y cells were incubated with glutamate or 6-hydroxidopamine and in order to evaluate neuroprotective effects of title compounds, cells were incubated with 0.1, 1 and 10 µM concentrations of **5b**,**d** for 1 h before adding to the cells the neurotoxins glutamate or 6-hydroxydopaminet riluzole, taken as reference drug, was tested as well. . Results demonstrated that all tested compounds exerted neuroprotection against glutamate-induced injury in a concentration-dependent fashion against glutamate-induced injury (Figure 4A); 10 µM or 0.01 µM were the most effective concentrations for 5b-d or riluzole, respectively, since cells recovery that occur was the highest observed (65-70%)..

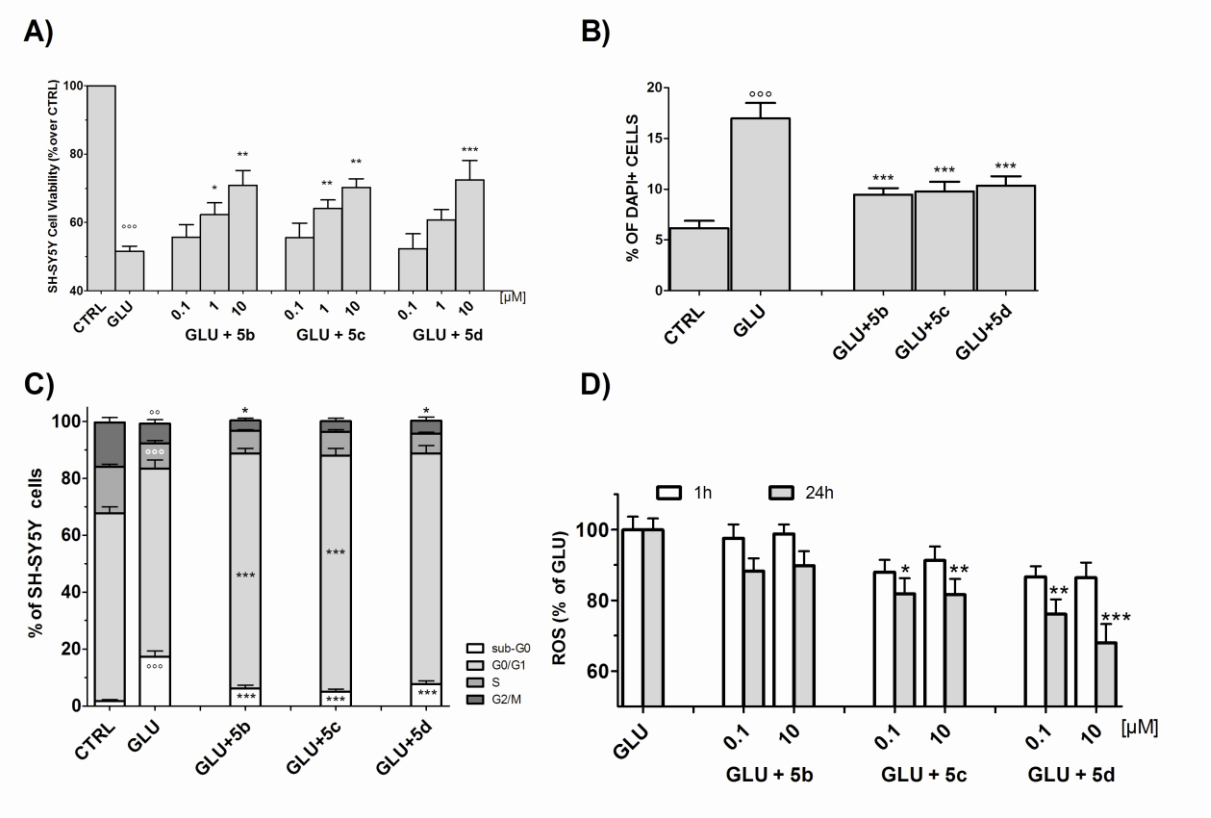

Figure 4. Effects of 1 h pretreatment with **5b**, **5c**, and **5d** (0.1-10 μM) on glutamate (GLU)-induced cytotoxicity (50 mM for 24 h) in SH-SY5Y cells. (A) Cell viability assessed by MTT assay. (B) Percentage of cells in the subG$_0$/G$_1$ (apoptotic) phase determined by flow cytometry after propidium iodide staining. (C) DAPI staining quantitative analysis. (D) Intracellular ROS production determined by means of the peroxide-sensitive fluorescent probe DCFH-DA and expressed as percent inhibition of intracellular ROS produced by GLU. Data are specified as mean ± SEM of 4 independent experiments (triplicate or quadruplicate were performed in each experiment). Statistical evaluation was performed by means of ANOVA followed by Dunnet post test. °°° $p < 0.001$ *vs* CTRL. *$p < 0.05$, ** $p < 0.01$, *** $p < 0.001$ *vs* GLU.

It should be noted that in this experimental model the concentrations of **5b-d** necessary for the neuroprotective effect were orders of magnitude greater than that of riluzole. This however was not the case of rat brain slices in which the novel derivatives-mediated neuroprotectionwas observed at concentration close or even lower than that of riluzole (see Table 1). This suggest that the presence of non-neuronal cellular elements as well as neurotransmitter interactions typical of a tissue context, is crucial for neuroprotection and could hamper in some way the effects of riluzole but not those of **5b-d**. Changes in SH-SY5Y cell cycle was also assessed. As illustrated in Figure 4B, the percent of sub-G_0/G_1 hypodiploid cells was significantly increased after glutamate challenge (+17.4 ± 1.9%, $p < 0.001$ vs CTRL), while those in the S and G_2/M phase were decreased. Interestingly, the pretreatment with selected compounds at 10 μM concentration significantly reduced the percentage of cells in sub G_0/G_1, and at the same time, it increased or left unchanged that in G_0/G_1 or in S phase, respectively.

SH-SY5Y morphological analysis was in agreement with previous data. The characteristic features of cell apoptosis induced by glutamate (i.e. cell tendency to round-up and detach from the culture plate, increased number of shrunken cell bodies with broken neurites, grade 2-3 toxicity) were, in fact, reverted by the selected compounds. This was further substantiated by data obtained by DAPI staining. The percent of apoptotic cells, which contained condensed and fragmented nuclear material, in fact, was dramatically increased after glutamate treatment (+16.9 ± 1.5 %, $p < 0.01$ vs CTRL) (Figure 4C). By contrast, the percent of cells displaying the fluorescence of the dye was significantly lower upon the pre-treatment with selected compounds (9-10%, $p < 0.01$ *vs* GLU (see also Figure S1 and S2 in the Supplementary Material). Finally, the effects of these compounds *per se* on SH-SY5Y cells viability were also tested. 24 h treatment with 10 μM of **5b-d** proved to be basically devoid of cytotoxic effects since only a slight reduction in cell viability (~10%, grade 0-1) was observed (data not shown).

ROS strongly contributes to cell death caused by oxidative glutamate toxicity and for this reason their intracellular formation was assessed by DCFH-DA assay. As shown in Figure 4D, the pre-treatment of SH-SY5Y cells with the above compounds elicited a concentration- and time-dependent

decrease in ROS production caused by glutamate. The maximal inhibitory effect was achieved at 10-μM for both **5c** and **5d** (24 h), at which concentration a reduction of about 20-40% in ROS formation was measured.

The neurotoxin 6-hydroxydopamine (6-OHDA), which is widely used as a neuronal damage inductor in experimental models of PD, has been reported to cause neuronal death by apoptosis, necrosis, or a combination of the two [34]. The ability of compounds **5b-d** and riluzole to revert 6-OHDA-induced injury was thus also tested in SH-SY5Y cells. As illustrated in Figure 5A, 6-OHDA (55 μM for 2 h) significantly decreased cell viability (47.6 ± 6.2%, $p < 0.01$), while a 1 h pretreatment of SH-SY5Y cells all the four compounds prevented 6-OHDA toxicity. The highest concentration used (10 μM for 5b-d, 0.01 for riluzole) was the most active in exerting neuroprotection, by causing an almost complete recovery in cell viability.

Furthermore, compounds **5b-d** reduced apoptotic cell death induced by 6-OHDA as determined by DAPI staining (Figure 5B). A high amount of DAPI-positive cells were found after treatment with 6OHDA, strongly suggesting the involvement of apoptosis in the neurotoxin-mediated SH-SY5Y death. On the contrary, compounds **5b-d** (10 μM) or riluzole (0.01 μM) reduced by about 20% the number of condensed or fragmented nuclei upon 6-OHDA treatment. Finally, to examine whether ROS formation mediated by 6-OHDA could be hampered by these compounds, H2DCF-DA assay was performed. In the presence of **5b-d** a concentration- and time-dependent reduction of intracellular ROS formation caused by the neurotoxin was observed (Figure 5C). Pretreatment of the cells with **5b-d**, indeed, afforded significant protection already at 0.1 μM, while maximum effects were achieved for all compounds at 10 μM.

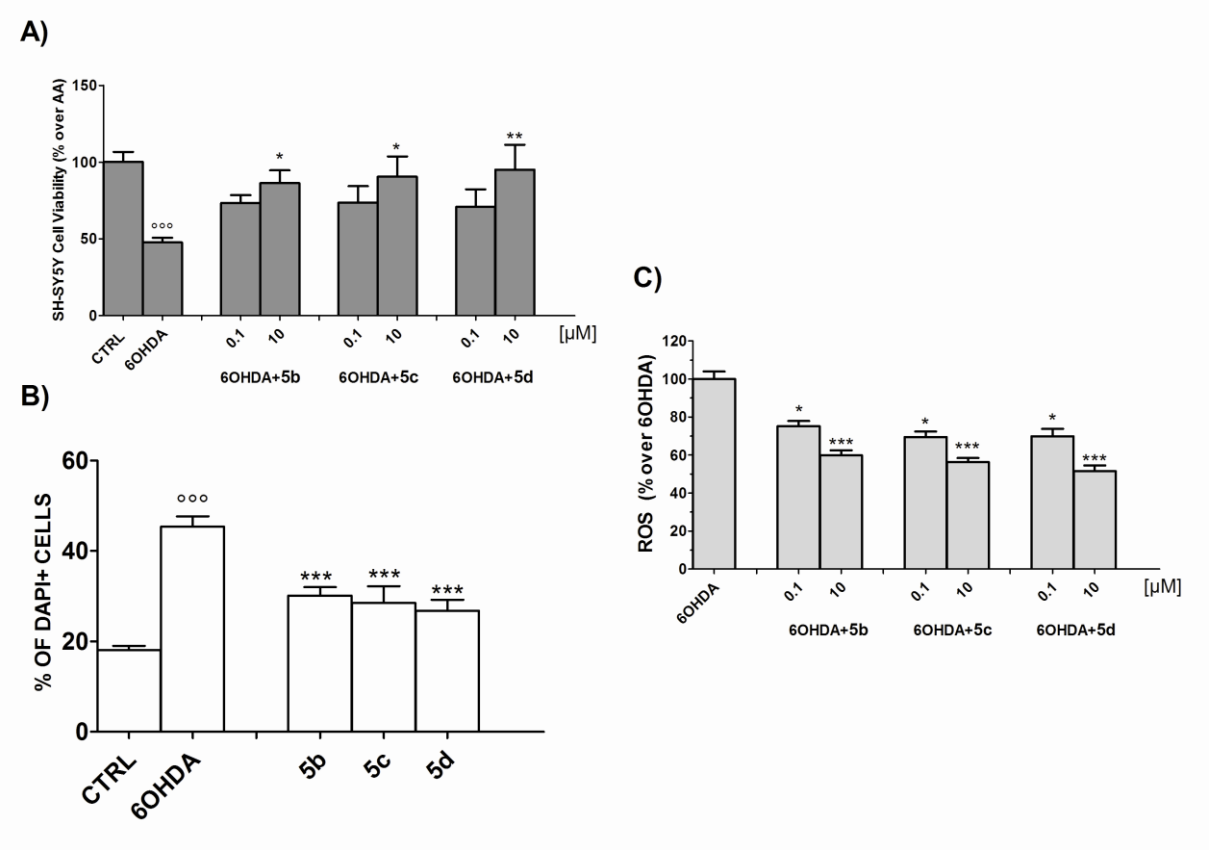

Figure 5. Effects of 1 h pretreatment with **5b**, **5c**, and **5d** (0.1-10 μM) on 6-hydroxydopamine (6-OHDA)-induced cytotoxicity (55 μM for 2 h) in SH-SY5Y cells. (A) Cell viability assessed by MTT assay. (B) DAPI staining quantitative analysis performed after treatment with 10 μM derivatives. (C) Intracellular ROS production determined by means of the peroxide-sensitive fluorescent probe DCFH-DA and expressed as the percent of inhibition of intracellular ROS produced by 6-OHDA. Data are specified as mean ± SEM of 4 independent experiments (triplicate or quadruplicate were performed in each experiment). Statistical evaluation was performed by means of ANOVA followed by Dunnet post test. °°° $p < 0.001$ *vs* CTRL. * $p < 0.05$, ** $p < 0.01$, *** $p < 0.001$ *vs* 6-OHDA.

2.3. Effects of compounds 5c and 5d on neuronal voltage-dependent Na^+ and Ca^{2+} currents

As already discussed elsewhere [2022], compound **1** inhibited voltage-dependent Na^+ currents by a mechanism in which stabilized the inactivated state of the Na^+ channels, representing an important basis of its neuroprotective action. Moreover, in peripheral sensory neurons [35] and cortical neurons

[22] **1** has also been proven to exert inhibitory effects on high-voltage-activated (HVA) Ca^{2+} channels. The inhibition of voltage-dependent Ca^{2+} influx under conditions of metabolic distress and depolarization could contribute to reduce the level of glutamate release, thus partly justifying the effects of **1** and compounds **5c** and **5d**. Accordingly, the activity of **5c** and **5d** on neuronal voltage-dependent Na^+ and Ca^{2+} currents and the comparison of the results with thos found for **1** has been performed.

Patch-clamp recordings [36] of voltage-dependent Na^+ currents were accomplished employing neurons of rat piriform cortex layer II in brain slices as an experimental model (see the Experimental Section for all details on the patch-clamp experiments). Differently from acutely dissociated neurons (see below), this preparation allowed for optimal Na^+ current stability, as required to evaluate the activity of the drugs examined. The transient Na^+ current (I_{NaT}) was studied by applying a current-voltage (*I/V*) protocol consisting of 19 ms depolarizing step pulses at −75 to 20 mV in 5 mV increments, starting from a holding potential of −80 mV (not shown). During drug application, I_{NaT} amplitude was also monitored by repetitively commanding (once every 10 s) a single 19 ms step at −20 mV (Figure 6C, D). **5c** or **5d** was applied through the bath perfusion at 50 μM.

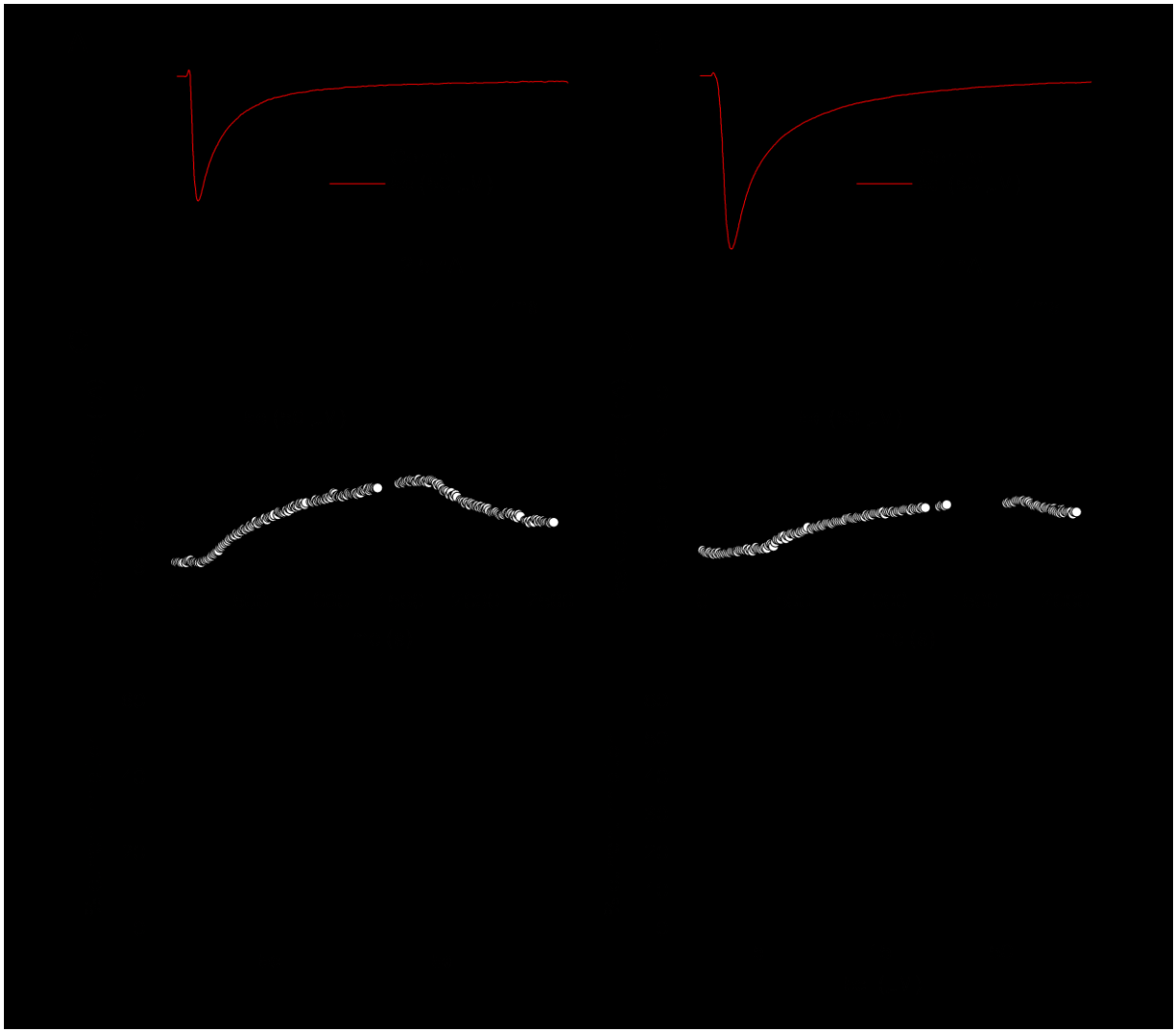

Figure 6. Effects of benzothiazine derivatives **5c** and **5d** on I_{NaT} amplitude. (A, B). Currents recorded in two representative neurons (cell E8722 in A; cell B8711 in B), at the test potential of V_p + 20 mV, under control conditions and during application of 50 μM **5c** (A) or **5d** (B). Arrows indicate the starting time of the depolarizing pulse. (C, D). Time course of the effects of benzothiazine compounds on I_{NaT} in two representative neurons (cell B8722 in A; cell B8710 in B). Drugs were applied, for the time interval indicated by horizontal bars, through the general perfusion. (E) Average percentages of I_{NaT} peak-amplitude inhibition induced by the benzothiazine compounds. n = 9 (**5c**) and 5 (**5d**). (F) Average percentages of I_{NaT} peak amplitude inhibited by **5c** at three different concentrations (5, 15 and 50 μM). n = 5, 4 and 9, respectively.

After a saturating effect on the I_{NaT} amplitude was reached, the drug's effect was quantified by measuring I_{NaT} inhibition at a voltage level equal to the *I/V* peak plus 20 mV (Figure 6A, B), rather than at the peak itself, to minimize the consequences of space-clamp artifacts [37]. 50 μM **5c** reduced I_{NaT} amplitude by 51.9 ± 2.1% (n = 9), whereas **5d** had a much weaker effect (15.9 ± 8.5% inhibition, n = 5) (Figure 6E). These effects were compared with the 51.6% inhibition exerted by **1** at 50 μM, as reported elsewhere for the same experimental conditions [22]. The effects of both **5c** and **5d** were partially reversible (Figure 6C, D). Since the effect of 50 μM **5d** on I_{NaT} amplitude was markedly and significantly smaller than that of the same concentration of **1** (p = 0.015), the activity of the former drug on Na^+ currents was not further characterized, and the investigation was focused on the effects of **5c**. The effects of this compound on Na^+ currents were examined also at two other concentrations of the drug, 5 and 15 μM. Figure 6F shows the concentration-dependence of the inhibition caused by **5c** on I_{NaT} amplitude. Based on these data, it can be inferred that the IC_{50} of the inhibitory effect induced by **5c** is very similar to that observed for **1** [22].

The ability of **5c** to modify the voltage dependence of I_{NaT} inactivation was then characterized and compared with that of **1**. The currents recorded in a representative neuron in the absence and in the presence of 15 μM of compound **5c** in response to the application of a steady-state inactivation protocol are illustrated in Figure 7B. Figure 7C shows the steady-state inactivation plots obtained from the same experiment: it can be seen that **5c** induced a marked shift of inactivation voltage dependence in the negative direction. Fitting of experimental data with single Boltzmann functions (Figure 7C, continuous lines) revealed that, at 15 μM, **5c** induced a negative shift of the inactivation function $V_{½}$ on average by 11.8 ± 2.4 mV (from –58.4 ± 1.6 mV to –70.4 ± 4.3 mV, n = 5): this compares with a –15.5 ± 0.4 mV shift induced by 15 μM of **1** under the same experimental conditions [22]. The slope coefficient of the inactivation function, instead, was not significantly modified (from 5.7 ± 0.2 mV to 6.3 ± 0.8 mV; p = 0.4, t test for paired data), whereas the maximal current amplitude was reduced, on average, by 24.2 ± 7.4% (n = 5): this reduction was statistically significant (p < 0.01).

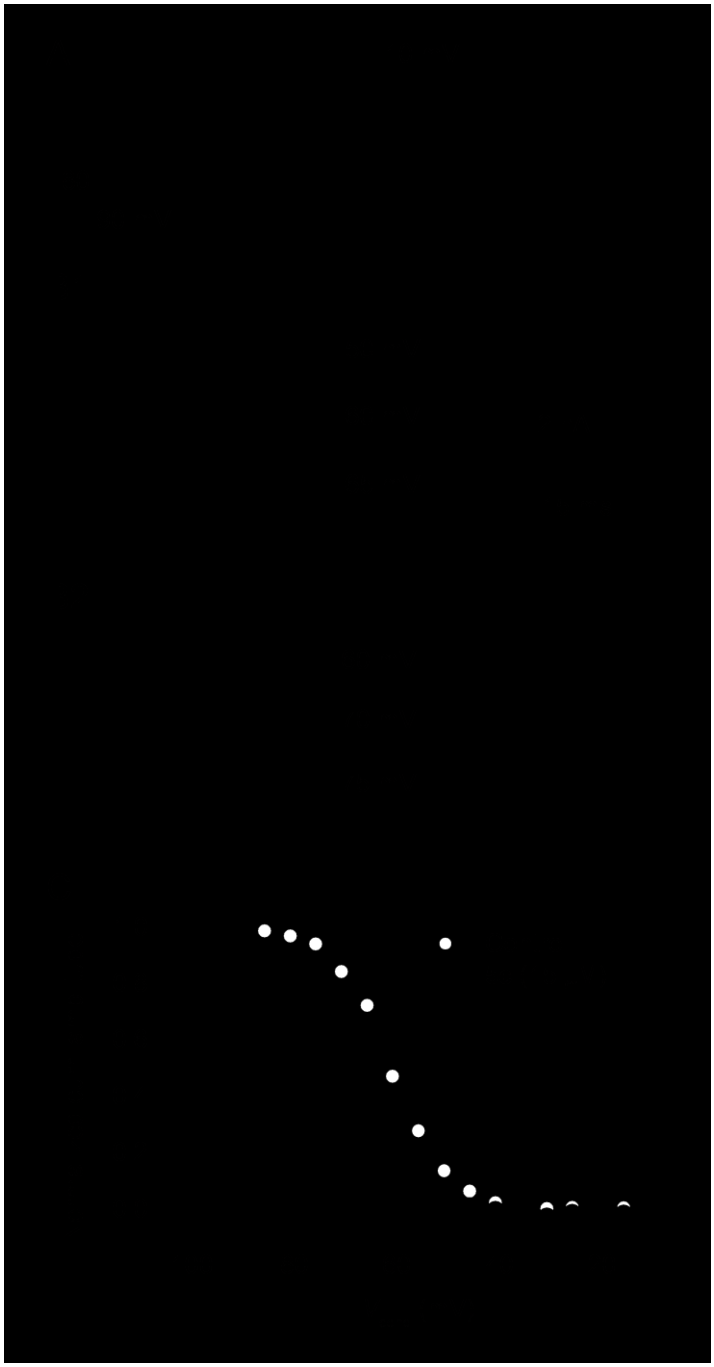

Figure 7. Compound **5c** induces a prominent negative shift in the steady-state inactivation curve of I_{NaT}. (A) Voltage-clamp protocol applied to study the voltage dependence of I_{NaT} steady-state inactivation. (B) Currents recorded in a representative neuron (cell A8731) in response to the protocol shown in A under control conditions and during application of 15 μM **5c**. The currents recorded at some significant conditioning potential levels (V_{cond}) are indicated by arrows. (C) Plots of the voltage dependence of I_{NaT} steady-state inactivation for the currents shown in panel B. Peak-current values

measured for the various V_{cond}s have been normalized for the maximal value observed in each condition, and plotted as a function of V_{cond}. Both plots have been fitted with a single Boltzmann function (continuous lines). Fitting parameters were: $V_{½}$ = –60.2 mV, k = 5.4 mV (control); $V_{½}$ = –71.5 mV, k = 5.2 mV (**5c**).

Similarly to **1** [22], **5c** also inhibited the persistent component of the Na^+ current (I_{NaP}) much more pronouncedly than I_{NaT}. The drug's effects on the I_{NaP} recorded in two representative neurons are illustrated in Figure 8. Compound **5c** reduced the peak amplitude of the I_{NaP} elicited by a 2 s depolarizing ramp protocol by 70.7 ± 5.2% at the concentration of 5 μM (n = 5), by 77.0 ± 6.9% at 15 μM (n = 5), and by 91.8 ± 3.6% at 50 μM (n = 4). These percent inhibition values were much, and significantly, greater than those observed for I_{NaT} amplitude ($p < 0.005$ for all three concentrations examined; t test for paired data). The inhibitory effects of **5c** on I_{NaP} amplitude were not significantly different from those observed for the same concentrations of **1** ($p > 0.25$ both at 15 μM and 50 μM; t test for unpaired data). Moreover, the selective inhibitory effect of **5c** on I_{NaP}, as compared to I_{NaT}, was already evident during the application of relatively brief (19 ms) step depolarizations (Figure 8C), indicating that the effect of **5c** on I_{NaP}, similarly to that of **1** [38], is a kinetically fast one.

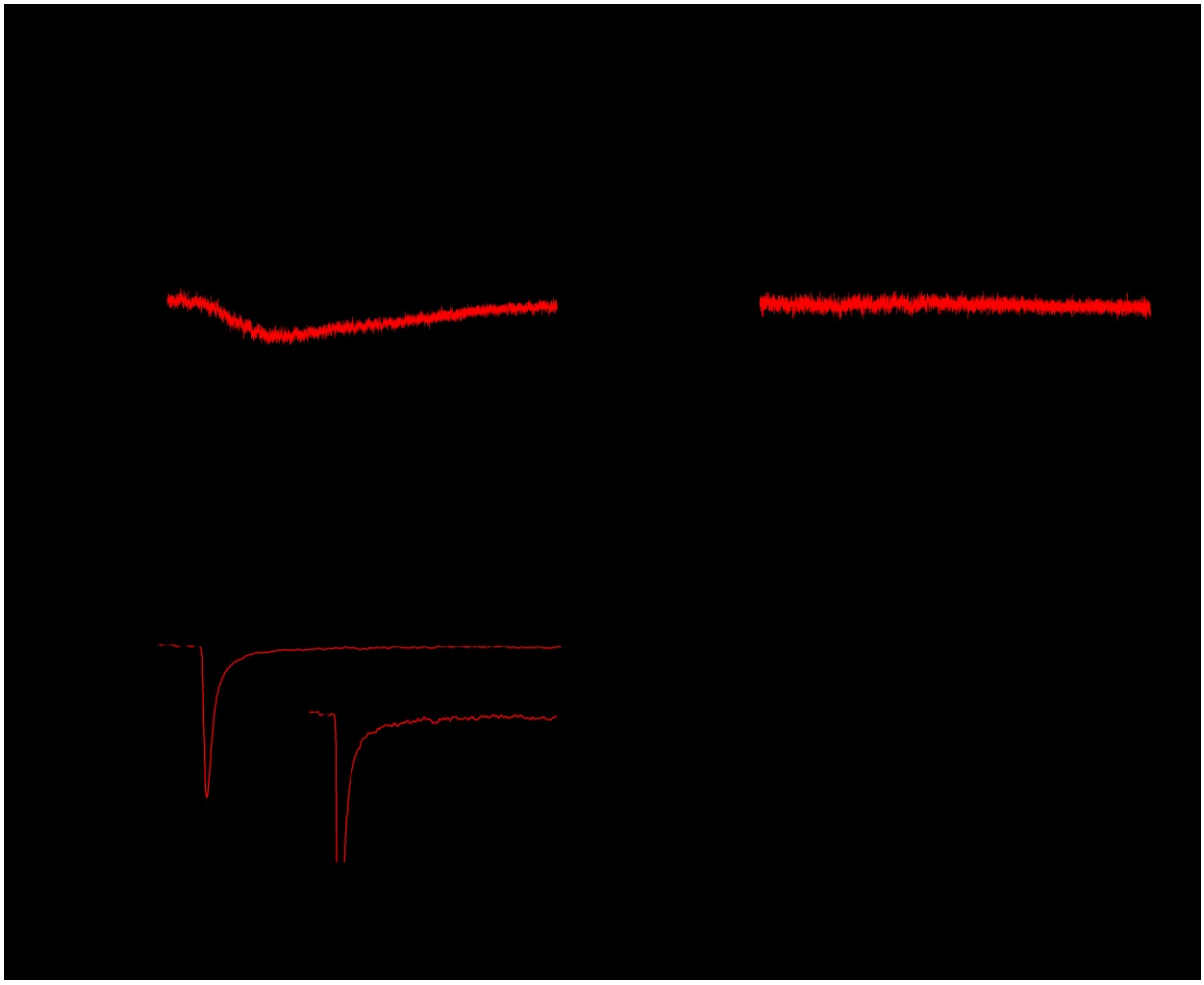

Figure 8. Compound **5c** potently inhibits I_{NaP}. (A, B) Currents (A2, B2) recorded in response to the ramp protocol applied to activate I_{NaP} (A1, B1) in two representative neurons (cell A8731 in A1; cell B8723 in B2) under control conditions and during application of 15 μM or 50 μM **5c**. The currents shown are TTx-subtracted and are plotted as a function of command potential. (C) The inhibition induced by 15 μM of **5c** on the transient and persistent components of the voltage-activated Na^+ current recorded in response to a 19 ms depolarizing voltage pulse at 0 mV. The inset shows, over an expanded amplitude scale, a highlight of the persistent currents recorded during the late phase of the depolarizing pulse. Note that even during such relatively short a depolarization **5c** inhibited the persistent current component much more prominently than the early, transient component. Same cell as in panel A. (D) Average effects of **5c** at three different concentrations (5, 15 e 50 μM) on the peak amplitude of I_{NaP} (evoked by the slow ramp protocol). Bars represent the average values of residual

I_{NaP} amplitude observed in the presence of **5c**, expressed as percent of control I_{NaP} amplitude. n = 5 (5 mM), 4 (15 μM) and 4 (50 μM).

A summary of the average values of percent inhibition induced by **5c** and **5d**, and by **1** for comparison, at the various concentrations tested, on the transient and persistent components of the voltage-dependent Na^+ current is provided by Table 2.

Table 2. Average values of the percent inhibition induced by compounds **5c** and **5d** on the amplitude of the transient and persistent components of the voltage-dependent Na^+ current.

Compounds	**Concentration (μM)**	**Percent inhibition**	
		I_{NaT}	I_{NaP}
1[a]	15	39.4 ± 7.1 (4)	87.3 ± 4.3 (4)
	50	51.6 ± 5.6 (6)	94.8 ± 9.0 (3)
5c	5	26.4 ± 7.2 (5)	70.7 ± 5.2 (5)
	15	36.0 ± 10.0 (4)	77.0 ± 6.9 (5)
	50	51.9 ± 2.1 (9)	91.8 ± 3.6 (4)
5d	50	15.9 ± 8.5 (5)	n. a.

[a]Data for **1** were taken from Ref. [22], are also given for comparison. Numbers of observations are indicated between parentheses. n.a., not available.

Voltage-dependent Ca^{2+} currents were evaluated in acutely dissociated neurons from rat piriform cortex layer II [39], in which they proved to be highly stable and optimal clamp conditions could be achieved. Ba^{2+} was used instead of Ca^{2+} as the charge carrier, and Ba^{2+} currents (I_{BaS}) were recorded. High-voltage-activated (HVA) currents were elicited by commanding depolarizing step or ramp protocols starting from a conditioning potential of −60 mV. **5c** and **5d** were applied to the recorded

neuron using a focal perfusion system [39]. The effects of compounds **5c** and **5d** on HVA currents were monitored by repetitively commanding (once every 7 s) a voltage-clamp protocol consisting of a 40 ms depolarizing ramp from −60 to +30 mV, which returned an "instantaneous" *I/V* relationship for total HVA currents (see Figure 9C-E). This instantaneous *I/V* closely matched that obtained with standard step *I/V* protocols (not shown, but see Ref. [22]). Current amplitude was measured at the peak of the instantaneous *I/V*.

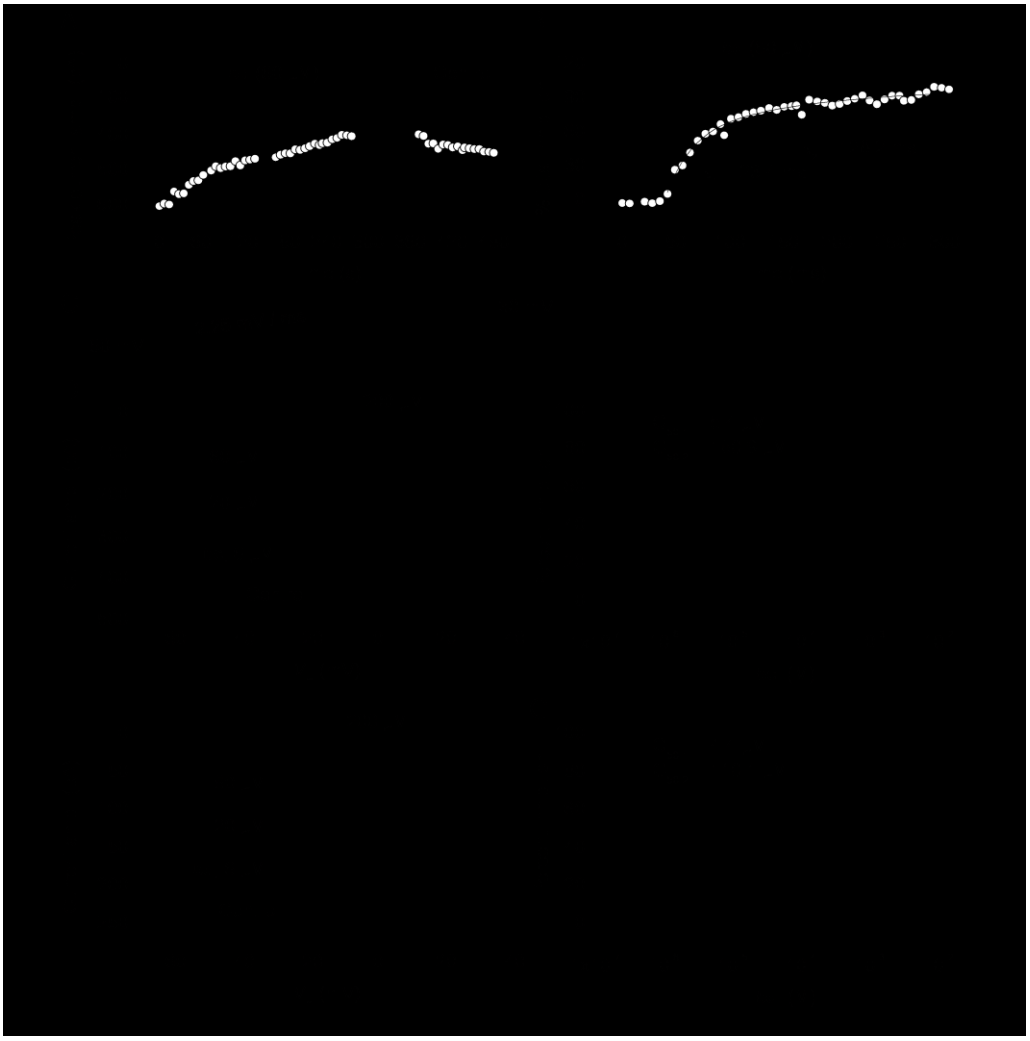

Figure 9. Compounds **5c** and **5d** inhibit neuronal HVA Ca^{2+} currents. (A) Time course of I_{Ba} amplitude changes in response to the application of 60 μM of **5d** in a representative neuron (cell C7517). Each data point represents the peak amplitude of a Ba^{2+} current (I_{Ba}) evoked by the ramp protocol depicted in panel C. **5d** was applied, for the time interval indicated by the black horizontal bar, via focal perfusion. Note the reversibility of the drug effect after wash out. (B) Average plot of the

time course of inhibition induced by **5d** (60 μM) on I_{Ba} amplitude. In each cell, peak I_{Ba} amplitude values have been used to calculate, for each data point, the quantity $[1 + (I_{Ba} - I_{ss}) / (I_0 - I_{ss})]\times100$, where I_{ss} is the current level observed after the development of a saturating effect of the drug, and I_0 is current amplitude before drug application: this quantity represents therefore the total inhibition percentage observed over time in that cell. The values thus obtained were then mediated among cells (n = 7). The average plot has been fitted with a double exponential function, with the following fitting parameters: A_1 = –51.3, τ_1 = 23.4 ms, A_2 = –41.3, τ_2 = 128.2 ms. (C) Ramp voltage-clamp protocol applied to evoke "instantaneous" *I/V* relationships for I_{Ba}s. (D, E) I_{Ba}s recorded in two representative neurons (cell B7O22 in D; cell C7515 in C) in response to the protocol illustrated in panel C under control conditions and in the presence of increasing concentrations of **5c** (D) and **5d** (E). (F, G) Concentration-dependence plots of percent inhibition induced by **5c** (F) and **5d** (G) on I_{Ba} amplitude. Single data points represent the average of values obtained from 4 (F) and 7 (G) cells. Data points have been fitted with the sum of two Hill functions (continuous lines). Fitting parameters were: A_1 = 33.0%, $IC_{50\text{-}1}$ = 5.4 μM, n_1 = 2.0, A_2 = 67.0%, $IC_{50\text{-}2}$ = 180.9 μM, n_2 = 1.0 (**5c**); A_1 = 22.7%, $IC_{50\text{-}1}$ = 4.4 μM, n_1 = 2.0, A_2 = 77.3, $IC_{50\text{-}2}$ = 110.1 μM, n_2 = 1.8 (**5d**).

Application of benzothiazine derivatives **5c** and **5d** *via* focal perfusion caused an inhibitory effect on barium current (I_{Ba}) peak amplitude with a biphasic time course (Figure 9A). Indeed, after activation of the drug's local perfusion an initial, fast reduction of the current was observed, followed by a further, slower reduction phase which required 3-4 min to reach a plateau level. As shown in Figure 9B, the average plot of the time course of inhibition could be properly fitted with a double exponential function, with time constant values that for **5d** were 23.4 ms and 128.2 ms. The effect of both drugs was partly reversible after wash out (n = 12) (Figure 9A).

The concentration-dependence of the effect of benzothiazine derivatives on I_{Ba} maximal amplitude is illustrated in Figure 9D-G. In both cases, the average concentration-dependence plots

were best fitted by the sum of two Hill functions, with IC_{50} values of 5.4 μM and 180.9 μM for **5c**; and 4.4 μM and 110.1 μM for **5d**. These results suggest that the action of benzothiazine derivatives on HVA channels is due to their interaction with at least two distinct binding sites.

On the contrary, reference compound **1** showed a single IC_{50} value of 34.2 μM along with a n_{Hill} value 0.82 [22], thus suggesting that its activity is due to the interaction with single binding site. Similarly to 1 [22], the inhibitory effect of **5c** and **5d** on I_{Ba} amplitude was not voltage-dependent, since the percentage of inhibition was constant over the range of test potentials explored to activate I_{Ba}s (–50 to +30 mV; not shown). This will be documented and discussed in more depth elsewhere.

Overall, the above results indicate that compound **5c** does exert major inhibitory effects on both voltage-activated Na^+ currents and HVA Ca^{2+} currents over a concentration range superimposable with that over which its *in vitro* neuroprotective effects were observed. Compound **5d** was likewise effective in inhibiting HVA Ca^{2+} currents, but much less so as far as voltage-dependent Na^+ currents are concerned.

2.4. Structure-activity relationships (SAR)

Although in the absence of a clear mechanism of action of the most active compounds, we have tried to extract from the biological results some information about structure-activity relationships (SAR) concerning the molecular modifications taken into consideration. Two different series of benzothiazines (**5**,**6** and **7**) have been designed as superior homologues of **1**. In particular, single point changes have been made to benzothiazole scaffold with the aim to understand which part can play a critical role.

Data from Table 1 showed how only 4*H*-3,1-benzothiazines **5b-d**, and to a lesser extent compounds **5a**, **7a**, **7d**, and **15**, based on the same N-C(S)-N skeleton of the parent compound, are able to elicit a better neuroprotective activity as compared to **1** itself. On the other hand, the inclusion of the

N-C(C-S)-N skeleton in the cyclic system of 2*H*-1,4-benzothiazine **6**, yields a series of compounds that proved to be inactive (For further details see Figure S3).

The insertion of a methylene group between the aromatic ring and the S atom in the 4*H*-3,1-benzothiazines **5b-d** allows one to obtain molecules less rigid without modifying the three-dimensional arrangement of N-C(S)-N atoms, typical of the riluzole system. For 2*H*-1,4-benzothiazine **6**, instead, the methylene insertion creates a structure more flexible, suggesting that a rigid skeleton constitutes the main pharmacophoric requirement to obtain novel active compounds able to protect against excitotoxic insult.

Regarding the substituent on the aromatic ring, it can be inferred that the presence of trifluoromethoxy group in position 6 of the ring does not seem to be essential for the neuroprotective activity: in fact, unsubstituted **5b-d** turned out to be the most active compounds within the series.

As mentioned before, we introduced amidine (**5-7**) or thiourea (**6**) moieties with the aim to evaluate whether the amino group is directly involved in the biological activity. Biological data from Table 1 show that thiourea derivative (**6**) is completely inactive, whereas amidine derivatives (**5-7**) proved active only in the absence of OCF_3 group. The contemporary presence of OCF_3 group along with the disubstituted amidine moiety in position 2 of the ring leads to inactive compounds due to a dramatic modification of the electrostatic distribution of the molecular surface (data not shown). Probably, trifluoromethoxy group as a long-range electron-withdrawing substituent [40] is able to considerably decrease the basicity of amidine moiety causing a perturbation of pK_a that can modify the binding affinity properties of the molecules. Furthermore, by means of the suitable alkyl substituents at the amidine nitrogen it is possible to modulate compounds' lipophilicity, a parameter required for a good binding affinity to the target protein. Obviously, this seems not be true for **1** and 4*H*-3,1-benzothiazine **15** in which the absence of the lipophilic amidine moiety is fully or partially compensated by OCF_3 group leading to an active and a moderately active compound, respectively.

Furthermore, in comparison with the inactive thiourea derivative **6**, the presence of disubstituted amidine moiety in 2-position of the most effective benzotiazines **5b-d** seems to be crucial in reverting OGD/R-induced LDH and glutamate release, with compounds **5c** and **5d** showing a wider efficacy window than **1**. As a whole, the transformation of the scaffold of **1** enlarging the benzothiazole nucleus to have 4*H*-3,1-benzothiazines decorated with the suitable lipophilic amidine moiety still leads to novel agents endowed with neuroprotective properties.

As far as the activity of the novel compounds on voltage-dependent Na^+ channels is concerned, compound **5c** was the one that showed the highest potency as an inhibitor of voltage-activated Na^+ currents, since it maintained a similar activity on the transient and persistent current components (I_{NaT} and I_{NaP}) as **1**. Compound **5d**, instead, proved to be markedly less effective at the same concentrations. Based on these results, it can be concluded that the substitution of benzothiazole ring of **1** with 4*H*-3,1-benzothiazine nucleus affords the preservation of pharmacological activity of **1** on voltage-gated Na^+ channels, as long as the aliphatic residues of acetamidine group are not too extended.

3. Conclusions

Amidine and thiourea derivatives **5-7** were synthesized, and their ability to counteract the excitotoxic cascade was evaluated. In an *in vitro* protocol of ischemia/reperfusion injury, 4*H*-3,1-benzothiazines **5b-d** significantly attenuated neuronal injury showing to be the most effective derivatives in reverting OGD/R-induced LDH and glutamate release in a concentration range between 0.1 and 25 μM. The same concentration-dependent neuroprotective effects were also observed in the human neuroblastoma cell line SH-SY5Y, commonly used to study neurotoxicity. Compounds **5b-d** counteracted apoptosis and ROS formation caused by the treatment with glutamate or 6-hydroxydopamine, two experimental models for excitotoxic- or oxidative stress-mediated injury.

Compound **5c** proved to maintain basically the same activity of **1** on the transient and persistent current components (I_{NaT} and I_{NaP}) of neuronal voltage-dependent Na^+ currents. On the contrary compound **5d** was markedly less effective at the same concentrations. Compound **5c** was able to exert a pronounced inhibitory effect on glutamate release limiting neuronal death much more effectively than previously reported benzothiazole compounds **2-4** [22]. This fact may be explained, at least in part, by the high potency with which **5**, differently from above-cited compounds, interferes with the function of voltage-gated Na^+ channels Differently from benzothiazole derivatives [22], **5c** and **5d** also proved effective as a HVA Ca^{2+}-channel inhibitors over a concentration range at least partly compatible with that of their neuroprotective effects. Indeed, the concentration-dependence plots of **5c** and **5d** effects on HVA I_{Ba} amplitude revealed the presence of an inhibitory component characterized by a relatively high potency, with IC_{50} of 4-5 μM and effective concentration levels very similar to those observed for neuroprotective effects.

Our results suggest that 4*H*-3,1-benzothiazine derivatives inhibit HVA Ca^{2+} channels in a contration-dependent manner interacting with at least two binding sites (contrary to compound 1 that likely interacts with one site [22]. Moreover, the fact that the inhibitory effect of these compounds developed with a biphasic time course indicates the existence of two distinct mechanisms of action

characterized by different time kinetics, one of which relatively slow. It is therefore possible that 4*H*-3,1-benzothiazine derivatives activate multiple mechanisms converging on HVA Ca^{2+} channels, thus inducing their inhibition. One of these mechanisms (probably the one developing with the slowest kinetics) could depend on the activation of G proteins, as previously suggested for the action of **1** on Ca^{2+} channels in dorsal-root ganglion neurons [35].

4. Experimental Section

4.1 Chemistry

Melting points were determined in open capillaries on a Gallenkamp apparatus and are uncorrected. Merck silica gel 60 (70-230 or 230-400 mesh) was used for column chromatography. Merck TLC plates, silica gel 60 F_{254} were used for TLC. ^{1}H NMR spectra were recorded with Bruker AC 200 spectrometer in the indicated solvents (TMS as internal standard): the values of the chemical shifts are expressed in ppm and the coupling constants (*J*) in Hz. Mass spectra were recorded on either a ThermoFinnigan LCQ-Deca or an Agilent 1100 LC/MSD. Purity of compounds **5a-f**, **6**, and **7a-f**, was assessed by RP-HPLC and was found to be higher than 95%. An Agilent 1100 Series system equipped with a Zorbax Eclipse XDB-C8 (4.6 x 150 mm, 5 μm) column was used in the HPLC analysis with methanol-water (80:20) as the mobile phase at a flow rate of 1.0 mL/min. UV detection was achieved at 254 nm.

4.1.1. 2-Amino-4H-3,1-benzothiazine (16) [28]

A mixture of 2-aminobenzylalcohol **13** (2.0 g, 16 mmol) in concentrated HCl (10 mL) was heated at 100 °C for 15 min in a sealed vial. The resulting precipitate was filtered and washed with diethyl ether to give **14** as a white solid that was solubilized in isopropanol (20 mL) and treated with thiourea (1.3 g, 17 mmol). The mixture was refluxed for 20 h, the solvent was removed under reduced pressure and the residue diluted with H_2O, made alkaline with 2 N NaOH (pH = 10), and extracted with CH_2Cl_2. The organic phase was washed with water to neutrality, dried over sodium sulfate, filtered, and concentrated under reduced pressure. The residue was purified by flash-chromatography with ethyl acetate/petroleum ether (1:1 v/v) as the eluent to give **16** as a light yellow solid (1.7 g, yield 64%.). Re-crystallization from EtOH gave an analytical sample melting at 132-135 °C. ^{1}H NMR ($CDCl_3$): 3.90 (s, 2H), 5.09 (br s, 2H), 7.00-7.12 (m, 3H) 7.20-7.28 (m, 1H). MS (ESI): *m/z* 165 ($M + H^+$). Due to its apparent instability compound **17** was transformed into the correspondent oxalate which after a cautious washing with dry diethyl ether gave a white solid melting at 178-182 °C.

4.1.2. 3-Amino-2H-1,4-benzothiazine (21) [29]

A mixture of 2-aminothiophenol **20** (1.6 mL, 15 mmol) in NaOH 25% (p/v) (10 mL) and chloroacetonitrile (0.95 mL, 15 mmol) in CH_2Cl_2 (20 mL) was stirred at room temperature in the presence of a catalytic amount of tetrabutylammonium hydrogen sulphate (0.51 g, 1.5 mmol). After 20 hours, the organic layer was separated dried over sodium sulfate, filtered, and concentrated under reduced pressure. The residue was dissolved in ethanolic hydrochloric acid (5%) (20 mL) and refluxed for 2 h. The solvent was removed under reduced pressure and the resulting solid was dissolved in water, washed with $CHCl_3$, made alkaline with concentrated NH_4OH (pH = 9.0) and extracted with $CHCl_3$. The organic layer was dried over sodium sulfate, filtered, and concentrated under reduced pressure. The obtained residue was purified by flash-chromatography with ethyl acetate/Et_3N (8:2 v/v) as eluent to obtain compound **21** as a light-yellow solid (0.80 g, yield 32%). Re-crystallization from ethyl acetate gave an analytical sample melting at 168-172 °C. ^{1}H NMR ($CDCl_3$): 3.18 (s, 2H), 4.38 (br s, 2H), 6.89-7.25 (m, 4H). MS (ESI): *m/z* 165 ($M + H^+$). Due to its apparent instability compound **21** was transformed into the correspondent oxalate which after a cautious washing with dry diethyl ether gave a white solid melting at 182-184 °C.

4.1.3. N-[4-(Trifluoromethoxy)phenyl]-pivaloylamide (9).

To a solution of 4-(trifluorometoxy)-aniline **8** (1.0 g, 5.6 mmol) and Et_3N (0.71 mL, 5.1 mmol) in dry CH_2Cl_2 (15 mL) cooled at 0 °C, pivaloyl chloride (0.73 mL, 5.9 mmol) was added dropwise. The reaction mixture was stirred for 18h at room temperature, poured into ice-water and extracted with CH_2Cl_2 (3 x 20 mL). The combined organic extracts were dried over Na_2SO_4, filtered and concentrated under reduced pressure to give **9** as white solid (1.1 g, yield 75%). Re-crystallization from *n*-hexane gave **9** as colorless needles (m. p. 104-107 °C). ^{1}H NMR ($CDCl_3$): 1.30 (s, 9H), 7.15 (d, J = 8.8, 2H), 7.33 (br s, 1H), 7.53 (d, J = 9.2, 2H). MS (ESI): *m/z* 262 ($M + H^+$).

4.1.4. N-[2-Formyl-4-(trifluoromethoxy)phenyl]-pivaloylamide (10).

t-butyllithium (1.7 M in pentane) (8.1 mL, 13.9 mmol) was added dropwise to a solution of pivaloyl amide **9** (1.5 g, 5.7 mmol) in dry THF (50 mL) cooled at -75 °C. After 1 h, the mixture was treated with DMF (0.44 mL, 5.7 mmol) and stirred at the same temperature for additional 45 min, then allowed to warm up to room temperature . After 20 min, the mixture was poured in ice-water. The organic layer was washed with 4 N HCl and brine, dried over Na_2SO_4, filtered and concentrated under reduced pressure. The residue was purified by flash-chromatography with CH_2Cl_2/petroleum ether (1:1 v/v) as eluent to obtain compound **11** as a colorless oil (1.2 g, yield 72%). ^{1}H NMR ($CDCl_3$): 1.34 (s, 9H), 7.43-7.50 (m, 2H), 8.86 (d, *J* = 9.0, 1H), 9.90 (s, 1H), 11.30 (br s, 1H), MS (ESI): *m/z* 290 ($M + H^+$).

4.1.5. N-[2-Hydroxymethyl-4-(trifluoromethoxy)phenyl]-pivaloylamide (11).

A solution of compound **10** (1.2 g, 4.1 mmol) in absolute EtOH (20 mL) cooled at 0 °C was treated with $NaBH_4$ (0.19 g, 4.9 mmol). The mixture was stirred for 15 min at 0 °C and at room temperature for additional 30 min. The solvent was concentrated under reduced pressure and the residue was diluted with H_2O and extracted with $CHCl_3$ (3x20 mL). The combined organic extracts were dried over Na_2SO_4, filtered and concentrated under reduced pressure to give **11** as colorless solid (1.2 g, yield 90%). Re-crystallization from *n*-hexane gave an analytical sample melting at 71-73 °C. ^{1}H NMR ($CDCl_3$): 1.30 (s, 9H), 2.24 (t, *J* = 5.9, 1H), 4.68 (d, *J* = 5.9, 2H), 7.03 (m, 1H), 7.16 (m, 1H), 8.15 (d, *J* = 8.9, 1H), 8.86 (br s, 1H). MS (ESI): *m/z* 315 ($M + Na^+$).

4.1.6. 2-Amino-6-trifluoromethoxy-4H-3,1-benzothiazine (15).

To a solution of compound **11** (0.35 g, 1.2 mmol) in dioxane (30 mL) cooled at 0 °C, HCl 37% (4 mL) was cautiously added. The mixture was heated at 80 °C for 4 h, and then diluted with isopropanol (20 mL) and added of thiourea (0.14 g, 1.8 mmol). The resulting reaction mixture was refluxed for 20 h and then concentrated under reduced pressure. The residue was diluted with H_2O, made alkaline with 2

N NaOH (pH = 9) and extracted with CH_2Cl_2 (3x15 mL). The combined organic extracts were dried over Na_2SO_4, filtered and concentrated under reduced pressure. The resulting residue was purified by flash-chromatography with ethyl acetate/petroleum ether (1:1 v/v) as eluent to give **15** as light yellow (0.25 g, yield 84%). Re-crystallization from EtOH gave an analytical sample melting at 115-118 °C. ^{1}H NMR ($CDCl_3$): 3.87 (s, 2H), 5.16 (br s, 2H), 6.97-7.11 (m, 3H). MS (ESI): *m/z* 249 ($M + H^+$).

4.1.7. 2-[2-Amino-5-(trifluoromethoxy)phenylthio]-acetonitrile (18).

A suspension of 2-amino-6-trifluoromethoxybenzothiazole **1** (1.8 g, 7.7 mmol) in 10 N NaOH (30 mL) was refluxed under a slow stream of nitrogen until the suspension turned to a clear solution. Then, a mixture of chloroacetonitrile (0.48 mL, 7.7 mmol) in CH_2Cl_2 (50 mL) and tetrabutylammonium hydrogen sulphate (0.26 g, 0.77 mmol) were added. The reaction mixture was stirred for 18 h at room temperature, the organic layer was then separated, washed with water, dried over Na_2SO_4 and filtered. The solvent was removed under reduced pressure and the residue was purified by flash-chromatography with petroleum ether/ethyl acetate (1:1 v/v) as eluent to give **18** as a brown oil (1.1 g, yield 58%). ^{1}H NMR ($CDCl_3$): 3.45 (s, 2H), 4.44 (br s, 2H), 6.74 (d, J = 8.8, 1H), 7.10 (m, 1H), 7.39 (m, 1H). MS (ESI): *m/z* 249 ($M + H^+$).

4.1.8. 3-Amino-7-trifluoromethoxy-2H-1,4-benzothiazine (19).

A solution of **18** (0.70 g, 2.82 mmol) in EtOH with HCl 5% (20 mL) was heated under reflux for 2 h. The solvent was concentrated under reduced pressure and the residue diluted with H_2O. The aqueous layer was washed with $CHCl_3$, made alkaline with concentrated NH_4OH (pH = 9) and the resulting precipitate was extracted with $CHCl_3$. The organic layer was dried over Na_2SO_4, filtered and concentrated under reduced pressure to give **19** as a light yellow solid (0.45 g, yield 64%, m.p. 94-96 °C). ^{1}H NMR ($CDCl_3$): 3.14 (s, 2H), 5.04 (br s, 2H), 6.92-7.10 (m, 3H). MS (ESI): *m/z* 249 ($M + H^+$).

4.1.9. General Procedure for the Synthesis of Acetamidines (5a-f, 7a-f).

To a solution of $POCl_3$ (4.9 mmol) in dry toluene (20 mL), cooled at 0 °C, the suitable acetamide (2.7 mmol) was added. After stirring under argon for 30 min at room temperature 2-amino- or 3-amino-benzothiazine (**15**, **16**, **19** or **21**) (2.4 mmol) was added. The reaction mixture was refluxed for 3h, cooled at room temperature and poured into ice-water. Then, the mixture was made alkaline with a solution of NaOH 2 N in water up to pH = 9 and extracted with $CHCl_3$. The organic layer was washed with H_2O, dried over Na_2SO_4, filtered and concentrated under reduced pressure. The resulting residue was purified by flash-chromatography with the indicated solvent as eluent to give the expected acetamidines (**5a**-**f**, **7a**-**f**).

4.1.10. N'-(4H-3,1-benzothiazin-2-yl)-N-methylacetamidine (5a).

Title compound was obtained as a light yellow solid starting from compound **16** and purified with ethyl acetate as eluent (yield 40%). ^{1}H NMR ($CDCl_3$): 2.16 (s, 3H), 3.04 (s, 3H), 3.94 (s, 2H), 7.00-7.08 (m, 3H), 7.17-7.024 (m, 1H), 11.90 (br s, 1H). MS (ESI): *m/z* 220 ($M + H^+$). Due to its instability compound **5a** was transformed into the correspondent oxalate which after a cautious washing with dry diethyl ether gave a solid melting at 110-113 °C dec.

4.1.11. N'-(4H-3,1-benzothiazin-2-yl)-N,N-dimethylacetamidine (5b).

Title compound was obtained as a light yellow oil starting from compound **16** and was purified with ethyl acetate as eluent (yield 63%). ^{1}H NMR ($CDCl_3$): 2.20 (s, 3H), 3.06 (s, 6H), 3.99 (s, 2H), 7.06-7.12 (m, 2H), 7.16-7.27 (m, 2H). MS (ESI): *m/z* 234 ($M + H^+$). Due to its instability compound **5b** was transformed into the correspondent oxalate which after a careful washing with dry diethyl ether gave a solid melting at 154-157 °C dec.

4.1.12. N'-(4H-3,1-benzothiazin-2-yl)-N,N-diethylacetamidine (5c).

Title compound was obtained as a yellow oil starting from compound **16** (1.2 mmol) and purified with petroleum ether-ethyl acetate (1:1 v/v) as eluent (yield 38%). ^{1}H NMR ($CDCl_3$): 1.18 (t, *J* = 7.2, 6H), 2.19 (s, 3H), 3.42 (br s, 4H), 3.97 (s, 2H), 7.01-7.07 (m, 2H), 7.14-7.27 (m, 2H). MS (ESI): *m/z* 262 ($M + H^+$).

4.1.13. N'-(4H-3,1-benzothiazin-2-yl)-N,N-dipropylacetamidine (5d).

Title compound was obtained as a light yellow oil starting from compound **16** (1.2 mmol), and purified with petroleum ether-ethyl acetate (1:1 v/v) as eluent (yield 54%). ^{1}H NMR ($CDCl_3$): 0.91 (t, *J* = 7.4, 6H), 1.61 (m, 4H), 2.19 (s, 3H), 3.29 (br s, 4H), 3.98 (s, 2H), 7.06-7.08 (m, 2H), 7.16-7.25 (m, 2H). MS (ESI): *m/z* 290 ($M + H^+$).

4.1.14. N,N-diethyl-N'-[6-(trifluoromethoxy)-4H-3,1-benzothiazin-2-yl]acetamidine (5e).

Title compound was obtained as a light yellow oil starting from compound **15** (1.2 mmol) and purified with petroleum ether-ethyl acetate (1:1 v/v) as eluent (yield 65%). ^{1}H NMR ($CDCl_3$): 1.24 (t, *J* = 7.3, 6H), 2.19 (s, 3H), 3.39 (br s, 4H), 3.95 (s, 2H), 6.95 (s, 1H), 7.04-7.18 (m, 2H). MS (ESI): *m/z* 346 ($M + H^+$).

4.1.15. N,N-dipropyl-N'-[6-(trifluoromethoxy)-4H-3,1-benzothiazin-2-yl]acetamidine (5f).

Title compound was obtained as a light yellow oil starting from compound **15** (1.2 mmol) and purified with petroleum ether-ethyl acetate (65:35 v/v) as eluent (yield 58%). ^{1}H NMR ($CDCl_3$): 0.89 (t, *J* = 7.3, 6H), 1.61 (m, 4H), 2.13 (s, 3H), 3.30 (br d, 4H), 3.93 (s, 2H), 6.93 (m, 1H), 7.04 (d, *J* = 9.6, 1H), 7.15 (d, *J* = 8.7, 1H). MS (ESI): *m/z* 374 ($M + H^+$).

4.1.16. N'-(2H-1,4-benzothiazin-3-yl)-N-methylacetamidine (7a).

Title compound was obtained as an orange-yellow solid starting from compound **21** and purified with ethyl acetate-Et_3N (9:1 v/v) as eluent (yield 28%). ^1H NMR ($CDCl_3$): 2.16 (s, 3H), 3.05 (s, 3H), 3.29 (s, 2H), 6.92-7.27 (m, 4H), 12.50 (br s, 1H). MS (ESI): *m/z* 220 ($M + H^+$). Due to its instability compound **7a** was transformed into the correspondent oxalate which after several washings with dry diethyl ether gave a solid melting at 164-166 °C dec.

4.1.17. N'-(2H-1,4-benzothiazin-3-yl)-N,N-dimethylacetamidine (7b).

Title compound was obtained as an orange oil starting from compound **21** and purified with ethyl acetate-Et_3N (95:5 v/v) as eluent (yield 26%). ^1H NMR ($CDCl_3$): 2.24 (s, 3H), 3.05 (s, 6H), 3.19 (s, 2H), 6.90-6.97 (m, 1H), 7.07-7.27 (m, 3H). MS (ESI): *m/z* 234 ($M + H^+$). Due to its instability compound **7b** was transformed into the correspondent oxalate which after several washings with dry diethyl ether gave a solid melting at 120-122 °C dec.

4.1.18. N'-(2H-1,4-benzothiazin-3-yl)-N,N-diethylacetamidine (7c).

Title compound was obtained as a green oil starting from compound **21** and purified with ethyl acetate as eluent (yield 16%). ^1H NMR ($CDCl_3$): 1.18 (t, J = 7.9, 6H), 2.26 (s, 3H), 3.18 (s, 2H), 3.44 (br s, 4H), 6.89-6.97 (m, 1H), 7.10-7.27 (m, 3H). MS (ESI): *m/z* 262 ($M + H^+$).

4.1.19. N'-(2H-1,4-benzothiazin-3-yl)-N,N-dipropylacetamidine (7d).

Title compound was obtained as a brown oil starting from compound **21** and purified with ethyl acetate as eluent (yield 9%). ^1H NMR ($CDCl_3$): 0.91 (t, J = 7.4, 6H), 1.63 (m, 4H), 2.26 (s, 3H), 3.23-3.29 (m, 6H), 6.89-6.97 (m, 1H), 7.07-7.27 (m, 3H). MS (ESI): *m/z* 290 ($M + H^+$).

4.1.20. N,N-diethyl-N'-[7-(trifluoromethoxy)-2H-1,4-benzothiazin-3-yl]acetamidine (7e).

Title compound was obtained as a yellow oil starting from compound **19** and purified with ethyl acetate as eluent (yield 34%). ^{1}H NMR ($CDCl_3$): 1.19 (t, *J* = 7.1, 6H), 2.27 (s, 3H), 3.18 (s, 2H), 3.25-3.47 (m, 4H), 6.96 (m, 1H) 7.11-7.20 (m, 2H). MS (ESI): *m/z* 346 ($M + H^+$).

4.1.21. N,N-dipropyl-N'-[7-(trifluoromethoxy)-2H-1,4-benzothiazin-3-yl]acetamidine (7f).

Title compound was obtained as an orange oil starting from compound **19** (1.2 mmol) and purified with petroleum-ethyl acetate (1:1 v/v) as eluent (yield 62%). ^{1}H NMR ($CDCl_3$): 0.91 (t, *J* = 7.3, 6H), 1.63 (m, 4H), 2.25 (s, 3H), 3.17-3.48 (m, 6H), 6.95 (d, *J* = 8.9, 1H), 7.11-7.20 (m, 2H). MS (ESI): *m/z* 374 ($M + H^+$).

4.1.22. 1-(4H-3,1-benzothiazin-2-yl)-3-propylthiourea (6).

To a solution of compound **16** (0.60 mmol) in dry toluene (20 mL) and Et_3N (0.10 mmol) stirred under argon atmosphere, the propyl isothiocyanate (0.84 mmol) was added dropwise. The reaction mixture was heated under reflux for 5 h and then cooled at room temperature. The solvent was removed under reduced pressure and the residue diluted with CH_2Cl_2. The resulting mixture was washed with H_2O, and the organic layer was dried over Na_2SO_4, filtered and concentrated under reduced pressure. The obtained residue was purified by washings with diethyl ether to obtain the compound 6 as a light yellow solid (yield 40%). Re-crystallization from ethyl acetate gave an analytical sample melting at 180-184°C. ^{1}H NMR (DMSO-d_6): 0.95 (m, 3H), 1.64 (m, 2H), 3.53 (m, 2H), 4.02 (s, 2H), 7.05-7.27 (m, 4H), 10.78 (s, 1H), 11.99 (br s, 1H). MS (ESI): *m/z* 266 ($M + H^+$).

4.2. Neuroprotection Experiments

4.2.1. Cell cultures

Human SH-SY5Y neuroblastoma cells were maintained in RPMI 1640 medium supplemented with 10% FBS, penicillin (100 U/ml), streptomycin (100 mg/ml), and L-glutamine (2 mM), in a humidified atmosphere of 95% air and 5% CO2 at 37 °C. Cells were sub-cultured when they were 70-80% confluent, fed twice each week and used for assays during exponential phase of growth.

4.2.2. Solution of drugs

Glutamate (GLU) solutions was prepared as already reported [41,42], while 6-OHDA was prepared immediately before use by dissolving the powder in 5 μM ascorbic acid solution previously gassed with nitrogen for 30 min. Stock solution of tested compounds were prepared in DMSO (1×10^{-1} M or 1×10^{-2} M) and diluted to the desired final concentration with PBS immediately before use. Final DMSO concentration in the samples was always lower than 0.01% and it did not affect investigated parameters.

4.2.3. Glutamate- or 6-hydroxydopamine-induced Injury in SH-SY5Y Cells

SH-SY5Y cells were seeded into 96-well plates (8 x 104 cells/mL, final volume 200 μL) and allowed to attach for 24 h. Afterward cells were pre-incubated with different concentration of tested compounds for 1 h and then GLU (50 mM for 24 h) or 6-OHDA (55 μM for 2 h) were added to the wells. These treatment were selected in preliminary experiments as they caused about 50% cell death [42]. After the injury, cell viability and apoptosis assays were performed as detailed below. Finally, the untreated group represented the control group (CTRL) which was treated with medium (GLU) or medium containing 5 μM ascorbic acid (6-OHDA).

4.3. Cell viability and morphological assay

3-(4,5-Dimethylthiazol-2-yl)-2,5-diphenyl-tetrazolium bromide (MTT) standard assay was used to assess cell viability [42]. In order to monitor changes in cell morphology caused by the treatment with neurotoxins, SH-SY5Y cells were observed under a phase-contrast light microscope and photographs were taken.

The results were evaluated using the grade scale, described in USP 28 (United States Pharmacopeia edition 2005) (grades 0-4) for assessment of the cytotoxic potential of tested materials, as follows: grade 0 - none reactivity (discrete intracytoplasmic granules, no cell lysis); grade 1 - slight reactivity (no more than 20% of the cells are round, loosely attached and without intracytoplasmic granules; occasional lysed cells are present); grade 2 - mild reactivity (no more than 50 % of the cells are round and devoid of intracytoplasmic granules, no extensive cell lysis and empty areas between cells); grade 3 - moderate (up to 70% of cells are rounded or lysed); grade 4 - severe (nearly complete destruction of the cells).

4.4. Apoptosis assays

Analysis of cell cycle and sub-G_0/G_1 population was used to check for cell apoptosis by means of flow cytometry. SH-SY5Y (2.5 x 105 cells/mL, final volume of 2 mL) were treated with selected compounds and then subjected to GLU or 6-OHDA treatment. After the toxic damage, cells were fixed with 70% ethanol (30 min at 4 °C) and then kept at -20 °C for at least 24 h.

DNA was extracted by using a FACScan flow cytometer through a 563-607 nm band-pass filter (BD Biosciences, San Jose, CA, USA). At least $1x10^4$ cells sample were acquired and the percentage of apoptotic cell (sub-G_0/G_1 peak) was quantified by using Cell Quest software (BD Biosciences, San Jose, CA, USA).

4.5. Intracellular ROS content

To detect the production of ROS, 2′, 7′-dichlorofluorescein diacetate (DCFH-DA)-based assay was used. Before any treatment, SH-SY5Y cells were loaded with the fluorescent probe (5 μM, 30 min) and then softly washed in PBS. Fluorescence was measured at 1 h or 24 h (wavelengths 485 nm excitation, and 535 nm emission). Antioxidant activity was expressed as the percent of inhibition of intracellular ROS produced by GLU or 6-OHDA treatment [39].

4.6. DAPI staining

DAPI (4',6-diamidino-2-phenylindole) staining kit (Life Tecnologies Italia, Monza, Italy) was used to check for cells with nuclei with fragmented and condensed, scored as apoptotic. Manufacturer's protocol, with minor modifications already described was used [42].

4.7. Rat brain cortical slices

All animal care and experimental protocols were approved by the Italian Department of Health (813/2015-PR) and conformed the EU Guidelines for the Care and the Use of Laboratory Animals (European Union Directive 2010/63/EU). The experimental protocols used were already reported [43, 44].

Briefly, cortical slices (400 μm) were prepared from Wistar rats (male, 250-300 g weight, Charles River Italia, Calco, Italy), and incubated in oxygenated artificial cerebrospinal fluid (ACSF, composition in mM 120 NaCl, 2.5 KCl, 1.3 $MgCl_2$, 1.0 NaH_2PO4, 1.5 $CaCl_2$, 26 $NaHCO_3$, 11 glucose, bubbled with 95% O_2 -5% CO_2, final pH 7.4, osmolality 285-290 mOsmol) for 1 h at room temperature.

Afterward slices were placed in flasks containing 2 ml ACSF and equilibrated for other 30 min at 37 °C. Oxygen glucose deprivation (OGD) was achieved by incubating slices into ischemic-ACSF (i.e. glucose-free ACSF added with 11 mM sucrose, continuously bubbled with a 95% N_2/ 5% CO_2 gas mixture) for 30 min. After the OGD phase, reoxygenation was reproduced by replacing the ischemic-

ACSF with fresh, oxygenated ACSF for an additional 90 min period. Neuroprotection exerted by tested compounds was investigated by adding them to the ACSF used during reoxygenation [43].

4.8. Assessment of brain slices injury

Brain slices injury was assessed by measuring the amount of both glutamate and LDH released into the ACSF during the entire reperfusion period as reported by Contarese *et al.* [43].

4.9. Data analysis

Data are expressed as mean ± SEM and were collected from at least 3 independent experiments, each run in quadruplicate. ANOVA (ordinary or repeated measures followed by Dunnett post test, GraphPad Prism version 5.04, GraphPad Software Inc., San Diego, CA, USA) was used to assess statistical significance at the significance level $p < 0.05$.

4.10. Patch-clamp experiments

Whole-cell, patch-clamp recordings were conducted in layer II pyramidal neurons of rat piriform cortex (PC), either in slices or after acute dissociation. All the procedures followed for obtaining piriform-cortex slices and acutely-dissociated neurons and for carrying out whole-cell recordings were exactly the same as described elsewhere (see Ref. [22]), and below they will be only briefly summarized. Young (P15-P22) Wistar rats of either sex were used, following a protocol that conformed with the rules established by the University of Pavia for the use of animals in experimental studies, in compliance with the guidelines of the Italian Ministry of Health, the national laws on animal research (d.l. 116/92), and the EU guidelines on animal research (N. 86/609/ CEE).

(i) Experiments on acute slices. 350 μm thick coronal sections of the anterior piriform cortex were cut under hypothermic conditions. During recordings, slices were perfused with an extracellular solution suitable for the isolation of Na^+ currents and containing: 100 mM NaCl, 26 mM $NaHCO_3$, 19.5 mM tetraethylammonium chloride (TEA-Cl), 3 mM KCl, 2 mM $MgCl_2$, 2 mM $CaCl_2$, 2 mM

$BaCl_2$, 0.5 mM $CdCl_2$, 4 mM 4-aminopyridine (4-AP), and 11 mM D-glucose (pH 7.4 by saturation with a 95% O_2/5% CO_2 mixture). Patch pipettes were filled with an intracellular solution containing 104 mM CsF, 50 mM TEA-Cl, 2 mM $MgCl_2$, 10 mM *N*-(2-hydroxyethyl) piperazine-*N0*-2-ethanesulfonic acid (HEPES), 10 mM ethylene glycol *bis*(β-aminoethyl ether) *N*,*N*,*N*′,*N*′-tetraacetic acid (EGTA), 2 mM adenosine 5′-triphosphate (ATP)-Na_2, and 0.2 mM guanosine 5′-triphosphate (GTP)-Na (pH adjusted to 7.2 with CsOH).

The general holding potential of voltage-clamp recordings was –80 mV. Current signals were low-pass filtered and digitized at cutoff and sampling frequencies of 5 and 50 kHz, respectively. Currents were always online leak subtracted via a P/4 routine. Tetrodotoxin (TTx) (Alomone Laboratories, Jerusalem, Israel) was applied in the bath with the superfusing solution at the end of all recordings, and currents recorded in the presence of 1 μM TTx were always subtracted from those recorded under control conditions and in the presence of drugs to abolish residual, unsubtracted capacitive and/or leakage currents.

(ii) Experiments on acutely dissociated neurons. A mechanical and enzymatic dissociation procedure described previously was applied [39]. After seeding in the recording chamber, cells were perfused with an oxygenated extracellular solution suitable for isolating Ba^{2+} currents conducted through Ca^{2+} channels, containing: 88 mM choline-Cl, 40 mM TEA-Cl, 3 mM KCl, 2 mM $MgCl_2$, 5 mM $BaCl_2$, 3 mM CsCl, 10 mM HEPES, 5 mM 4-AP, and 25 mM D-glucose (pH 7.4 with HCl). Patch pipettes were filled with an intracellular solution containing 78 mM Cs methanesulfonate, 40 mM TEA-Cl, 10 mM HEPES, 10 mM EGTA, 20 mM phosphocreatine di-Tris salt, 2 mM ATP-Na_2, and 20 units/mL creatine phosphokinase (pH adjusted to 7.2 with CsOH). Tight seals (> 5 GΩ) and the whole-cell configuration were obtained according to the standard technique [36]. All recording conditions were as previously described [39]. The general holding potential of voltage-clamp recordings was –70 mV. Current signals were filtered at 5 kHz and digitized at 50 kHz.

(iii) Drug Application. Concentrated (30 mM) stock solutions of **1** and compounds **5c** and **5d** were prepared in DMSO, divided into small aliquots, and stored at –20 °C. The aliquots were then

diluted to the final concentrations in one of the extracellular solutions described above. Preliminary control experiments indicated that DMSO had no significant effects on Ca^{2+} currents when applied at the same concentrations used to dissolve drugs in aqueous solution (0.02-0.67%, v/v). In experiments for recording Na^+ currents in slices, the drug-containing extracellular solution was applied through the bath perfusion. In experiments for recording Ca^{2+} currents in acutely dissociated neurons, drugs were applied through a local perfusion system described elsewhere [22].

(iv) Data Analysis. Whole-cell current signals were analyzed using Clampfit from pClamp version 8.2 (Axon Instruments, Union City, CA). Na^+ currents were normally refiltered off-line at 3.5 kHz. Current amplitude was measured at the peak of each tracing. Average values were expressed as arithmetic means ± SEM. Statistical significance was evaluated by applying the two-tail Student's *t* test for paired or unpaired data, as appropriate.

Supplementary material

Supplementary data associated with this article (Figures S1-S3, X-Ray Crystallography can be found, in the online version, at….

Abbreviation list

6-OHDA 6-hydroxydopamine; ACSF Artificial cerebrospinal fluid; AD Alzheimer's disease; ALS amyotrophic lateral sclerosis; CTRL control; DAPI 4',6-diamidino-2-phenylindole; DCFH-DA Dichloro-dihydro-fluorescein diacetate; DMF *N*,*N*-dimetilformammide; EGTA Ethylene glycol tetraacetic acid; GLU glutamate; H2DCF-DA 2',7'-dichlorodihydrofluorescein diacetate; HD Huntington's disease; HEPES (4-(2-hydroxyethyl)-1-piperazineethanesulfonic acid; HVA High-voltage-activated; L-NAME L-N^G-Nitroarginine methyl ester; LDH Lactate dehydrogenase; MEC minimal effective concentration; MTT 3-(4,5-dimethylthiazol-2-yl)-2,5-diphenyltetrazolium bromide; MW Molecular weight; NMDA N-methyl-D-aspartate; *n*NOS neuronal nitric oxide synthase; NO

Nitric oxide; OGD/R oxygen/glucose deprivation and reperfusion model ; PD Parkinson's disease ; RP-HPLC Reversed-phase high-performance liquid chromatography; ROS Reactive oxygen species; SEM standard error of measurement; TEA trimethylamine; THF tetrahydrofuran; TLC thin layer chromatography; TTx Tetrodotoxin.

Conflict of Interest

The authors declare no competing financial interest.

Acknowledgements

The authors wish to thank Rottapharm Biotech S.r.l. Monza, Italy for financial support. Dr Francesco Makovec and Prof. Fabio Fusi are kindly acknowledged for fruitful suggestions and encouragement during the experiments.

References

[1] http://epthinktank.eu/2013/07/17/neurodegenerative-diseases-in-the-workplace last access March 2015.
[2] R. Djaldetti, N. Lev, E. Melamed, Neuroprotection in progressive brain disorders, Isr Med Assoc J, 5 (2003) 576-580.
[3] A. Nieoullon, Neurodegenerative diseases and neuroprotection: current views and prospects, Journal of Applied Biomedicine, 9 (2011) 173-183.
[4] A. Mehta, M. Prabhakar, P. Kumar, R. Deshmukh, P.L. Sharma, Excitotoxicity: bridge to various triggers in neurodegenerative disorders, Eur J Pharmacol, 698 (2013) 6-18.
[5] S. Butini, K. Nikolic, S. Kassel, H. Bruckmann, S. Filipic, D. Agbaba, S. Gemma, S. Brogi, M. Brindisi, G. Campiani, H. Stark, Polypharmacology of dopaminereceptor ligands, Prog. Neurobiol. 142 (2016) 68e103.
[6] L. Ismaili, B. Refouvelet, M. Benchekroun, S. Brogi, M. Brindisi, S. Gemma, G. Campiani, S. Filipic, D. Agbaba, G. Esteban, M. Unzeta, K. Nikolic, S. Butini,J. Marco-Contelles, Multitarget compounds bearing tacrine- and donepezillike structural and functional motifs for the potential treatment of Alzheimer's disease, Prog. Neurobiol. (2016), http://dx.doi.org/10.1016/j.pneurobio.2015.1012.1003.
[7] E. Fernandez-Espejo, Pathogenesis of Parkinson's disease: prospects of neuroprotective and restorative therapies, Mol Neurobiol, 29 (2004) 15-30.
[8] R.M. Bonelli, G.K. Wenning, H.P. Kapfhammer, Huntington's disease: present treatments and future therapeutic modalities, Int Clin Psychopharmacol, 19 (2004) 51-62.
[9] O. Ates, S.R. Cayli, I. Gurses, A.B. Karabulut, N. Yucel, A. Kocak, C.O. Cakir, S. Yologlu, Do sodium channel blockers have neuroprotective effect after onset of ischemic insult?, Neurol Res, 29 (2007) 317-323.
[10] E. Benoit, D. Escande, Riluzole specifically blocks inactivated Na channels in myelinated nerve fibre, Pflugers Arch, 419 (1991) 603-609.

[11] T. Hebert, P. Drapeau, L. Pradier, R.J. Dunn, Block of the rat brain IIA sodium channel alpha subunit by the neuroprotective drug riluzole, Mol Pharmacol, 45 (1994) 1055-1060.
[12] J.H. Song, C.S. Huang, K. Nagata, J.Z. Yeh, T. Narahashi, Differential action of riluzole on tetrodotoxin-sensitive and tetrodotoxin-resistant sodium channels, J Pharmacol Exp Ther, 282 (1997) 707-714.
[13] C. Zona, A. Siniscalchi, N.B. Mercuri, G. Bernardi, Riluzole interacts with voltage-activated sodium and potassium currents in cultured rat cortical neurons, Neuroscience, 85 (1998) 931-938.
[14] M.W. Debono, J. Le Guern, T. Canton, A. Doble, L. Pradier, Inhibition by riluzole of electrophysiological responses mediated by rat kainate and NMDA receptors expressed in Xenopus oocytes, Eur J Pharmacol, 235 (1993) 283-289.
[15] A. Doble, The pharmacology and mechanism of action of riluzole, Neurology, 47 (1996) S233-241.
[16 D. Martin, M.A. Thompson, J.V. Nadler, The neuroprotective agent riluzole inhibits release of glutamate and aspartate from slices of hippocampal area CA1, Eur J Pharmacol, 250 (1993) 473-476.
[17] M.E. Frizzo, L.P. Dall'Onder, K.B. Dalcin, D.O. Souza, Riluzole enhances glutamate uptake in rat astrocyte cultures, Cell Mol Neurobiol, 24 (2004) 123-128.
[18] G. Bensimon, L. Lacomblez, V. Meininger, A controlled trial of riluzole in amyotrophic lateral sclerosis. ALS/Riluzole Study Group, N Engl J Med, 330 (1994) 585-591.
[19] H.M. Bryson, B. Fulton, P. Benfield, Riluzole. A review of its pharmacodynamic and pharmacokinetic properties and therapeutic potential in amyotrophic lateral sclerosis, Drugs, 52 (1996) 549-563.
[20] R.G. Miller, J.D. Mitchell, M. Lyon, D.H. Moore, Riluzole for amyotrophic lateral sclerosis (ALS)/motor neuron disease (MND), Cochrane Database Syst Rev, (2002) CD001447.
[21] M. Anzini, A. Cappelli, G. Caselli, A. Giordani, F. Makovec, L.C. Rovati, S. Vomero, Amidine, thiourea and guanidine derivatives of 2-aminobenzothiazoles and aminobenzothiazines for their use as pharmacological agents for the treatment of neurodegenerative pathologies, in, Google Patents, 2009.
[22] M. Anzini, A. Chelini, A. Mancini, A. Cappelli, M. Frosini, L. Ricci, M. Valoti, J. Magistretti, L. Castelli, A. Giordani, F. Makovec, S. Vomero, Synthesis and biological evaluation of amidine, guanidine, and thiourea derivatives of 2-amino(6-trifluoromethoxy)benzothiazole as neuroprotective agents potentially useful in brain diseases, J Med Chem, 53 (2010) 734-744.
[23] Y. Zhu, D. Nikolic, R.B. Van Breemen, R.B. Silverman, Mechanism of inactivation of inducible nitric oxide synthase by amidines. Irreversible enzyme inactivation without inactivator modification, J Am Chem Soc, 127 (2005) 858-868.
[24] M.M. Iravani, L. Liu, S. Rose, P. Jenner, Role of inducible nitric oxide synthase in N-methyl-d-aspartic acid-induced strio-nigral degeneration, Brain Res, 1029 (2004) 103-113.
[25] R.C. Babbedge, S.L. Hart, P.K. Moore, Anti-nociceptive activity of nitric oxide synthase inhibitors in the mouse: dissociation between the effect of L-NAME and L-NMMA, J Pharm Pharmacol, 45 (1993) 77-79.
[26] S.G. Kim, H.J. Kim, C.H. Yang, Thioureas differentially induce rat hepatic microsomal epoxide hydrolase and rGSTA2 irrespective of their oxygen radical scavenging effect: effects on toxicant-induced liver injury, Chem Biol Interact, 117 (1999) 117-134.
[27] F. Audiau, C. James, Medicaments containing 2-benzothiazolamine derivatives, compounds and their preparation, in, EP0374041 A1, 1990.
[28] D.R. Shridhar, K. Srinivasa Rao, Synthesis of Some New N-Benzothiazinyl-N'-aryl/pyridyl-thioureas as potential Anthelmintic Agents, Indian J. Chem., 20B (1981) 471-473.
[29] D.R. Shridhar, C.V. Reddy Sastry, O.P. Bansal, P. Pulla Rao, Synthesis & Biological Activity of Some New N-(2H-1,4-benzoxazin- & benzothiazin-3-yl)-N'-arylureas, Indian J. Chem., 25B (1986) 874-876.
[30] A.D. Jordan, C. Luo, A.B. Reitz, Efficient conversion of substituted aryl thioureas to 2-aminobenzothiazoles using benzyltrimethylammonium tribromide, The Journal of organic chemistry, 68 (2003) 8693-8696.

[31] L. Farkas, E. Kasztreiner, F. Andrasi, J. Borsi, J. Kosary, E. Csanyi, S. Elek, Thiazolylurea derivatives and process for the preparation thereof, (1976) Patent GB 1437895, 1431976e1437806-1437803. EC: C1437807D1437417/1437804; C1437807D1437417/1437814.
[32] A. Krishna, M. Biryukov, C. Trefois, P.M. Antony, R. Hussong, J. Lin, M. Heinaniemi, G. Glusman, S. Koglsberger, O. Boyd, B.H. van den Berg, D. Linke, D. Huang, K. Wang, L. Hood, A. Tholey, R. Schneider, D.J. Galas, R. Balling, P. May, Systems genomics evaluation of the SH-SY5Y neuroblastoma cell line as a model for Parkinson's disease, BMC Genomics, 15 (2014) 1154.
[33] S. Brogi, S. Butini, S. Maramai, R. Colombo, L. Verga, C. Lanni, E. De Lorenzi, S. Lamponi, M. Andreassi, M. Bartolini, V. Andrisano, E. Novellino, G. Campiani, M. Brindisi, S. Gemma, Disease-modifying anti-Alzheimer's drugs: inhibitors of human cholinesterases interfering with beta-amyloid aggregation, CNS Neurosci Ther, 20 (2014) 624-632.
[34] Y.M. Ding, J.D. Jaumotte, A.P. Signore, M.J. Zigmond, Effects of 6-hydroxydopamine on primary cultures of substantia nigra: specific damage to dopamine neurons and the impact of glial cell line-derived neurotrophic factor, J Neurochem, 89 (2004) 776-787.
[35] C.S. Huang, J.H. Song, K. Nagata, J.Z. Yeh, T. Narahashi, Effects of the neuroprotective agent riluzole on the high voltage-activated calcium channels of rat dorsal root ganglion neurons, J Pharmacol Exp Ther, 282 (1997) 1280-1290.
[36] O.P. Hamill, A. Marty, E. Neher, B. Sakmann, F.J. Sigworth, Improved patch-clamp techniques for high-resolution current recording from cells and cell-free membrane patches, Pflugers Arch, 391 (1981) 85-100.
[36] L. Castelli, M.J. Nigro, J. Magistretti, Analysis of resurgent sodium-current expression in rat parahippocampal cortices and hippocampal formation, Brain Res, 1163 (2007) 44-55.
[37] L. Castelli, M.J. Nigro, J. Magistretti, Analysis of resurgent sodium-current expression in rat parahippocampal cortices and hippocampal formation, Brain Res. 1163 (2007) 44-55.
[38] A. Urbani, O. Belluzzi, Riluzole inhibits the persistent sodium current in mammalian CNS neurons, Eur J Neurosci, 12 (2000) 3567-3574.
[39] J. Magistretti, L. Castelli, V. Taglietti, F. Tanzi, Dual effect of Zn2+ on multiple types of voltage-dependent Ca2+ currents in rat palaeocortical neurons, Neuroscience, 117 (2003) 249-264.
[40] E. Castagnetti, M. Schlosser, The trifluoromethoxy group: a long-range electron-withdrawing substituent, Chemistry, 8 (2002) 799-804.
[41] N. Croce, S. Bernardini, S. Di Cecca, C. Caltagirone, F. Angelucci, Hydrochloric acid alters the effect of L-glutamic acid on cell viability in human neuroblastoma cell cultures, J Neurosci Methods, 217 (2013) 26-30.
[42] C. Brizi, C. Santulli, M. Micucci, R. Budriesi, A. Chiarini, C. Aldinucci, M. Frosini, Neuroprotective Effects of Castanea sativa Mill. Bark Extract in Human Neuroblastoma Cells Subjected to Oxidative Stress, J Cell Biochem, 117 (2016) 510-520.
[43] A. Contartese, M. Valoti, F. Corelli, S. Pasquini, C. Mugnaini, F. Pessina, C. Aldinucci, G. Sgaragli, M. Frosini, A novel CB2 agonist, COR167, potently protects rat brain cortical slices against OGD and reperfusion injury, Pharmacol Res, 66 (2012) 555-563.
[44] F. Aiello, M. Badolato, F. Pessina, C. Sticozzi, V. Maestrini, C. Aldinucci, L. Luongo, F. Guida, A. Ligresti, A. Artese, M. Allara, G. Costa, M. Frosini, A. Schiano Moriello, L. De Petrocellis, G. Valacchi, S. Alcaro, S. Maione, V. Di Marzo, F. Corelli, A. Brizzi, Design and Synthesis of New Transient Receptor Potential Vanilloid Type-1 (TRPV1) Channel Modulators: Identification, Molecular Modeling Analysis, and Pharmacological Characterization of the N-(4-Hydroxy-3-methoxybenzyl)-4-(thiophen-2-yl)butanamide, a Small Molecule Endowed with Agonist TRPV1 Activity and Protective Effects against Oxidative Stress, ACS Chem Neurosci, (2016).

List of Figure Captions

Figure 1. Reference compounds.

Figure 2. Structures of target compounds **5-7**.

Figure 3. Effects of compounds **5b**, **5c** and **5d** on the release of glutamate and LDH induced by oxygen/glucose deprivation and reoxygenation (OGD/R) in rat cortical slices. Drugs were added to reoxygenation buffer used after OGD. Data are mean ± SEM of at least four different experiments. Statistical analysis was performed by applying ANOVA followed by a post hoc Dunnett test. °°°$p <$ 0.01 *vs* controls (CTRL). *$p < 0.05$, **$p < 0.01$, ***$p < 0.001$ *vs* OGD/R.

Figure 4. Effects of 1 h pretreatment with **5b**, **5c**, and **5d** (0.1-10 μM) on glutamate (GLU)-induced cytotoxicity (50 mM for 24 h) in SH-SY5Y cells. (A) Cell viability assessed by MTT assay. (B) Percentage of cells in the subG_0/G_1 (apoptotic) phase determined by flow cytometry after propidium iodide staining. (C) DAPI staining quantitative analysis. (D) Intracellular ROS production determined by means of the peroxide-sensitive fluorescent probe DCFH-DA and expressed as percent inhibition of intracellular ROS produced by GLU. Data are specified as mean ± SEM of 4 independent experiments (triplicate or quadruplicate were performed in each experiment). Statistical evaluation was performed by means of ANOVA followed by Dunnet post test. °°° $p < 0.001$ *vs* CTRL. *$p < 0.05$, ** $p < 0.01$, *** $p < 0.001$ *vs* GLU.

Figure 5. Effects of 1 h pretreatment with **5b**, **5c**, and **5d** (0.1-10 μM) on 6-hydroxydopamine (6-OHDA)-induced cytotoxicity (55 μM for 2 h) in SH-SY5Y cells. (A) Cell viability assessed by MTT assay. (B) DAPI staining quantitative analysis performed after treatment with 10 μM derivatives. (C) Intracellular ROS production determined by means of the peroxide-sensitive fluorescent probe DCFH-DA and expressed as the percent of inhibition of intracellular ROS produced by 6-OHDA. Data are specified as mean ± SEM of 4 independent experiments (triplicate or quadruplicate were performed in

each experiment). Statistical evaluation was performed by means of ANOVA followed by Dunnet post test. °°° $p < 0.001$ *vs* CTRL. * $p < 0.05$, ** $p < 0.01$, *** $p < 0.001$ *vs* 6-OHDA.

Figure 6. Effects of benzothiazine derivatives **5c** and **5d** on I_{NaT} amplitude. (A, B). Currents recorded in two representative neurons (cell E8722 in A; cell B8711 in B), at the test potential of V_p + 20 mV, under control conditions and during application of 50 μM **5c** (A) or **5d** (B). Arrows indicate the starting time of the depolarizing pulse. (C, D). Time course of the effects of benzothiazine compounds on I_{NaT} in two representative neurons (cell B8722 in A; cell B8710 in B). Drugs were applied, for the time interval indicated by horizontal bars, through the general perfusion. (E) Average percentages of I_{NaT} peak-amplitude inhibition induced by the benzothiazine compounds. n = 9 (**5c**) and 5 (**5d**). (F) Average percentages of I_{NaT} peak amplitude inhibited by **5c** at three different concentrations (5, 15 and 50 μM). n = 5, 4 and 9, respectively.

Figure 7. Compound **5c** induces a prominent negative shift in the steady-state inactivation curve of I_{NaT}. (A) Voltage-clamp protocol applied to study the voltage dependence of I_{NaT} steady-state inactivation. (B) Currents recorded in a representative neuron (cell A8731) in response to the protocol shown in A under control conditions and during application of 15 μM **5c**. The currents recorded at some significant conditioning potential levels (V_{cond}) are indicated by arrows. (C) Plots of the voltage dependence of I_{NaT} steady-state inactivation for the currents shown in panel B. Peak-current values measured for the various V_{cond}s have been normalized for the maximal value observed in each condition, and plotted as a function of V_{cond}. Both plots have been fitted with a single Boltzmann function (continuous lines). Fitting parameters were: $V_{½}$ = –60.2 mV, k = 5.4 mV (control); $V_{½}$ = –71.5 mV, k = 5.2 mV (**5c**).

Figure 8. Compound **5c** potently inhibits I_{NaP}. (A, B) Currents (A2, B2) recorded in response to the ramp protocol applied to activate I_{NaP} (A1, B1) in two representative neurons (cell A8731 in A1; cell B8723 in B2) under control conditions and during application of 15 μM or 50 μM **5c**. The currents

shown are TTx-subtracted and are plotted as a function of command potential. (C) The inhibition induced by 15 μM of **5c** on the transient and persistent components of the voltage-activated Na^+ current recorded in response to a 19 ms depolarizing voltage pulse at 0 mV. The inset shows, over an expanded amplitude scale, a highlight of the persistent currents recorded during the late phase of the depolarizing pulse. Note that even during such relatively short a depolarization **5c** inhibited the persistent current component much more prominently than the early, transient component. Same cell as in panel A. (D) Average effects of **5c** at three different concentrations (5, 15 e 50 μM) on the peak amplitude of I_{NaP} (evoked by the slow ramp protocol). Bars represent the average values of residual I_{NaP} amplitude observed in the presence of **5c**, expressed as percent of control I_{NaP} amplitude. n = 5 (5 mM), 4 (15 μM) and 4 (50 μM).

Figure 9. Compounds **5c** and **5d** inhibit neuronal HVA Ca^{2+} currents. (A) Time course of I_{Ba} amplitude changes in response to the application of 60 μM of **5d** in a representative neuron (cell C7517). Each data point represents the peak amplitude of a Ba^{2+} current (I_{Ba}) evoked by the ramp protocol depicted in panel C. **5d** was applied, for the time interval indicated by the black horizontal bar, via focal perfusion. Note the reversibility of the drug effect after wash out. (B) Average plot of the time course of inhibition induced by **5d** (60 μM) on I_{Ba} amplitude. In each cell, peak I_{Ba} amplitude values have been used to calculate, for each data point, the quantity $[1 + (I_{Ba} - I_{ss}) / (I_0 - I_{ss})]\times100$, where I_{ss} is the current level observed after the development of a saturating effect of the drug, and I_0 is current amplitude before drug application: this quantity represents therefore the total inhibition percentage observed over time in that cell. The values thus obtained were then mediated among cells (n = 7). The average plot has been fitted with a double exponential function, with the following fitting parameters: A_1 = –51.3, τ_1 = 23.4 ms, A_2 = –41.3, τ_2 = 128.2 ms. (C) Ramp voltage-clamp protocol applied to evoke "instantaneous" *I/V* relationships for I_{Ba}s. (D, E) I_{Ba}s recorded in two representative neurons (cell B7O22 in D; cell C7515 in C) in response to the protocol illustrated in panel C under control conditions and in the presence of increasing concentrations of **5c** (D) and **5d** (E). (F, G)

Concentration-dependence plots of percent inhibition induced by **5c** (F) and **5d** (G) on I_{Ba} amplitude. Single data points represent the average of values obtained from 4 (F) and 7 (G) cells. Data points have been fitted with the sum of two Hill functions (continuous lines). Fitting parameters were: A_1 = 33.0%, $IC_{50\text{-}1}$ = 5.4 μM, n_1 = 2.0, A_2 = 67.0%, $IC_{50\text{-}2}$ = 180.9 μM, n_2 = 1.0 (**5c**); A_1 = 22.7%, $IC_{50\text{-}1}$ = 4.4 μM, n_1 = 2.0, A_2 = 77.3, $IC_{50\text{-}2}$ = 110.1 μM, n_2 = 1.8 (**5d**).

List of Scheme Captions

Scheme 1. Reagents: (i) $(CH_3)_3CCOCl$, Et_3N, CH_2Cl_2; (ii) *t*-BuLi, dry THF, dry DMF; (iii) $NaBH_4$, absolute EtOH; (iv) HCl 37%, dioxane; (v) HCl 37%, sealed vial; (vi) NH_2CSNH_2, i-PrOH.

Scheme 2. Reagents: (i) NaOH 10 M; (ii) $ClCH_2CN$, $(Bu)_4N^+HSO_4^-$, NaOH 10 M, CH_2Cl_2; (iii) HCl/EtOH 5%; (iv) $ClCH_2CN$, $(Bu)_4N^+HSO_4^-$, NaOH 25%, CH_2Cl_2.

Scheme 3. Reagents: (i) NH_4SCN, $PhCH_2N(CH_3)_3Br_3$, CH_3CN.

Scheme 4. Reagents: (i) $CH_3CONR_1R_2$, $POCl_3$, dry toluene; (ii) R_1NCS, Et_3N, dry toluene. R_1 is defined in Figure 2.

List of Table Captions

Table 1. Effects of **1** and compounds **5e-f**, **6b**, **7a-d** and **15** on OGD and reperfusion-induced release of glutamate (GLU) and LDH in rat cortical brain slices.

Table 2. Average values of the percent inhibition induced by compounds **5c** and **5d** on the amplitude of the transient and persistent components of the voltage-dependent Na^+ current.

Running Title

Benzothiazines as neuroprotective agents